Tor Vergata University, Rome, Italy

GeoInformation PhD Programme

XVIII Cycle

Monitoring burned woodland by SAR and a scattering model

Tutor

Prof. Fabio Del Frate

PhD Candidate

Andrea Minchella

June 2006

ACKNOWLEDGEMENT

Firstly, I would like to thank my tutor Prof. Fabio Del Frate and the coordinator of PhD Geoinformation programme Prof. Domenico Solimini for all the support and the help, not only scientific, given to me during the PhD course. These three years have provided to me the possibility to enter more deeply in contact with the world of Remote Sensing and to understand how it is important for the life of our planet and our life. But besides to these more "philosophic considerations", I would like to mention some people with I have had the pleasure to meet and work together:

my PhD colleagues Ricardo Duca, Michele Iapaolo, Andrea Arturi, Andrea Radius, John Merryman Boncori, Chiara Solimini, Andrea Della Vecchia, Alessandro Burini, Cosimo Putignano, Pasquale Sellitto; the ESA staff Luigi Fusco, Maurizio Fea and Francesco Sarti who I met during my period as visiting scientist in ESA-Esrin; the mythic Prof. Emanuele Loret "the G.I.S drake", Fulvio Comandini and all the trainees of the G:I.S room; all the other Professors of the PhD programme, especially Prof. Giovanni Schiavon and Prof. Leila Guerriero;

A special thanks to Prof. Paolo Ferrazzoli and Andrea Dalla Vecchia for the helping into understanding some problematic related to the development of the model, to the research group of Prof. Fausto Manes of the Plant Biology department of "La Sapienza" University, Rome, in particular to Francesca Capogna and Silvia Anselmi, for the collaboration and the helpfulness to share their knowledge and data on the Castel Fusano site.

I thank my family, my father, my mother, my "little brother" Giorgio who have encouraged and sustained me for all the time.

At last, but first in my heart and in my thoughts, I would like to thank the most important person of my life, "my sweet half" Manuela.

Thanks to all for this experience!

Andrea

TABLES OF CONTENT

Chapter 1 State of the Art and Scope of this Work

1.1 Why to study burnt areas?

Mapping and monitoring fire-disturbed areas is very important for local resource and land management as well as global change research. Atmospheric gas emissions due to biomass burning and the long term post-fire biogenic gas emissions from the scarred landscape have important implications for climate change [1], [2]. To give an idea of the impact of fire in certain areas of the world, the example of the Russian boreal forest, which accounts for one of the largest reservoirs of terrestrial carbon [3], can be considered. In boreal forests, fire affects dramatically the flow of energy between the atmosphere and ground layer, and there is a dependence on the melting and formation of permafrost and the occurrence of fire, which in turn has a strong influence on the hydrology of these sites [4]. In particular, the Siberian boreal forest is considered a carbon sink but may become an important source of carbon dioxide if climatic warming predictions are correct. The forest is continually changing through various disturbance mechanisms such as insects, logging, mineral exploitation, and especially fires. About 16,000 forest fires occur in Russia every year, with an average annual area burned of 900,000 hectares [5]. Patterns of disturbance and forest recovery processes are important factors regulating carbon flux in this area [6]. Hence, the detection of fires and the assessment of their impacts on the vegetation are important to monitor, model and predict global climate change. From this point of view, the rate of biomass over burned areas is a crucial factor for the damage assessment related to a forest fire event. In some cases, the reforestation process is very fast and after few years the burned areas will be completely repopulated; in other cases such a process can take even decades so that the environmental and economic impact of the fire event is much stronger. The knowledge on the repopulation

capability over burned areas of different types of vegetation is so far sparse and limited to local experiences. Satellite data can alternatively offer the possibility of a more systematic investigation on the topic.

1.2 Use of Remote Sensing for fire monitoring

Since fires often affect large areas, Remote Sensing offers the most appropriate spatial and within-year temporal resolution to assess the impact of fire especially in remote areas difficultly accessible by man. Satellite images provide a means for monitoring the patterns, extent, and frequency of fire as well as any possible shifts in ecosystem types. Traditionally, researchers have focused on the utility of optical or thermal sensors for the mapping and monitoring of active fires and fire scars. The longest global record extends from only 1981 to the present, in the form of AVHRR imagery from the National Oceanic and Atmospheric Administration (NOAA) satellite series. Data from this source are widely available at spatial resolutions of 1, 4, and 8 km and temporal resolutions varying typically from daily coverage to 10-day or 18-day composites. The thermal data of the AVHRR sensors have been used for locating fires in real time, i.e., fire hot spots [7], [8]; the optical data for estimating burned area from one month to one year after the fire has occurred, i.e., recent fire scars [9]-[12]. A combination of both for monitoring wildfire evolution [13]. Similarly, thermal and optical data from more recent coarse-scale sensors are being used for hotspot detection (ATSR series [14] and MODIS [15]) and for recent fire scar mapping (ATSR series [16] and SPOT-VEGETATION [17], [18]), respectively. At higher spatial resolution, the optical sensor, Landsat Thematic Mapper (TM), has been used to map burned areas and fire severity [19], [20].

Hot spot detection relies on the difference between the heat of the observed fires and the relatively cold surroundings. The main algorithms that have been developed are either threshold based methods or contextual methods. A thorough review of hot spot detection algorithms is presented in [21]. A number of tests are normally required to remove false alarms caused, in particular, by sun glint, warm backgrounds, industry,

cloud reflection, and bright-scene objects. To date, a number of national and global active fire products derived from earth observation are available online (e.g., on the ATSR world fire atlas website, the World Fire Web website, and the MODIS Land Rapid Response System website). Hot spot products are obtainable from 1992, 1993, and 1995 to the present on a daily, 8–10 daily or monthly basis. The accuracy of fire detection from these products is low for fires of low intensity and can be hampered by false alarms and cloud cover.

Fire scar mapping using optical imagery exploits the differences observed in the spectral signatures between healthy forest canopy and forests destroyed or damaged by fire. Healthy green vegetation, including forests, typically absorbs light in the red (0.6–0.7 m) wavelengths (chlorophyll absorption), scatters light in the near infrared (NIR: 0.7–1.3 m) (intracellular scattering) and absorbs in the shortwave-infrared (SWIR: 1.4–1.8 m) (plant moisture absorption). After burning, more soil is exposed, and the whole or proportions of the forest will have been destroyed. This generally results in a spectral signature showing higher red, lower NIR, and higher SWIR reflectance values, although charcoal on the surface can temporarily lower the red signal. The Advanced Very High Resolution Radiometer (AVHRR) data, for example, were successfully used to determine area and location of Alaskan fire scars in the 1990 and 1991 fire seasons [10]. The 1.0 km resolution, bi-monthly composite, Normalized Difference Vegetation Index (NDVI) data were used for this study. The method developed relies on the detection and mapping of the reduced “greenness” (NDVI) immediately after a fire as well as the delayed “green up” the following spring. This method can only be used to detect fire scars in the first year after a fire because the rapid re-vegetation results in increased NDVI and a reduced ability to discriminate the burned areas. Typically, by the spring following a fire, mosses, liverworts, and herbaceous plants invade the charred landscape. This initial stage of development generally lasts from two to five years depending on the site and the burn severity [22]. The next stage is dominated by shrubs and lasts from years 5 to 25. The methods developed for optical imagery include the following:

- normalized difference vegetation index (NDVI) differencing;

- thresholding of single bands;
- thresholding of multiple bands and vegetation indexes;
- unsupervised image classification
- image segmentation.

Most of the methods listed produce reasonable results for estimating the extent of burned areas in the year that the fire occurred. The majority of the most successful methods use thresholding of a combination of bands and usually include brightness temperature. An algorithm that exploits features of the two approaches has been adopted for the production of GLOBSCAR, a global burned area product derived from ATSR-2 imagery. GLOBSCAR (www.geosuccess.net) is available from the European Space Agency. It shows monthly burned areas at 1 km resolution for the year 2000. The Joint Research Centre at Ispra (Italy) has also produced a 1-km global map of burnt areas for the year 2000 (GBA2000) from daily SPOT-VEGETATION Imagery. With respect to the large-area monitoring of older fire scars (i.e., areas burned more than one year prior to image acquisition) and their regeneration patterns, earth observation tools are not well developed. Nevertheless, [12] has shown that the SWIR band is critical to the detection of older forest fire scars. Canopy moisture content, to which SWIR is sensitive, may be linked to vegetation type and canopy structure. This may explain why, in the SWIR, older regenerating fire scars are distinguishable from the surrounding mature forests.

Nevertheless several techniques have been developed for using visible, infrared and thermal data to successfully detect and map active fires and burn scars, anyway, there are a number of problems associated with using optical satellite imagery. Spectral overlaps between fire scars and terrain shadows, water bodies, unburnt canopies, and vegetation in burnt areas create substantial difficulties in separating and discriminating fire classes [23]. Therefore most fire-mapping methods focus on the areas where vegetation distribution and topographic features are almost uniform. However, the greatest problem of this technology is the inability to penetrate cloud.

On the other event, space-borne radar has proved effective in monitoring and assessing the extent and severity of wild fires in the boreal forests of Alaska and in the tropical forests of Indonesia and research shows SAR has unique capabilities that may compliment and enhance multi-spectral techniques for fire scar monitoring.

Fire scars could be detected between 3 and 7 years in Alaska and Canada after the fire event with European Remote-Sensing Satellite (ERS) or Radarsat SAR data [24]. The backscatter of burnt forest detected by the ERS SAR was 3-6dB brighter than adjacent unburned forest. The reasons for this increase was the tree canopy removal, ground surfaces exposure and increased soil moisture [25]. These effects occurred only when the burnt area was wet such as in early spring, early autumn and after rainfall. Increased ground moisture is the dominant factor causing the enhanced backscatter from burnt forests. An increase in soil moisture after a fire is attributed to decreased surface albedo and melting of the permafrost layer as well as lowered evapotranspiration [26]. Bourgeau-Chavez *et al.* [24] compared the temporal variation of the visibility of fire scars in SAR images in Canada and found that the scars were bright after snowmelt in the spring, faded as the ground dried out and became bright again during rainfall and they also found season variations in fire scar visibility occurs globally, with the best season for fire scar detection being either spring or early autumn depending on the site. L-band data was found to be less sensitive to fire events in Alaskan and tropical forests [27], while C-band backscatter after a fire event decreased in tropical forests under dry conditions [28].

This effect was found to be strongest in a non-forest environment and related to moisture content of the ground surface: increased ground moisture is the dominant factor causing the enhanced backscatter from burned forests. The overall effects of fire on soil moisture are a function of fire severity, soil type and the presence or absence of permafrost.

However, layover and shadowing in steep mountainous regions, wetlands and seasonal conditions are the major factors disturbing the applicability of SAR imagery to detect fire scars [25]. Compositing multiple dates SAR or classifying the image

into positive and negative slopes were tried to solve the problem of layover and shadowing [25], [29].

1.3 Microwave electromagnetic modelling of vegetation

Many experimental results demonstrate that radar sensitivity to biomass extends over wide dynamic ranges of the backscatter coefficient σ^0 [30], [36]. However, the electromagnetic interaction effects producing this sensitivity need still to be more deeply understood and furthermore the backscatter coefficients are available only over a limited number of tree and vegetation species.

To this end, it is important to develop and test electromagnetic models, since they allow to investigate separately the σ^0 dependence on the various vegetation parameters. Models give a physical basis to experimental correlations between radar response and medium parameters, allow identification of the different scattering sources within the canopy and make it possible to carry out parametric investigations.

Concerning the forests, numerous models have been published in literature. The models differ principally in two respects: the characterisation of the forest and the calculation of its scattering properties.

They are generally based on the Radiative Transfer (RT) theory or on the Distorted Born Approximation (DBA). The RT theory describes the forest canopy as a homogeneous half space overlayed by an ensemble of discrete dielectric scatterers, representing vegetation elements, sparsely and randomly distributed so that the fields add incoherently. On the other hand, the Distorted Born Approximation is an analytical wave theory that includes information on both the amplitude and the phase of the scattered waves, calculating the total scattering by adding the complex scattered fields from all the elements.

In this work the attention is focused on two electromagnetic scattering models, which have been used for biomass retrieval: the Water Cloud model that is the simplified RT model with a single category of scatterers and the more complicated Tor Vergata

model in which the single scatterer behaviour is described by the complete bistatic scattering cross-section and whose some routines have been implemented.

1.4 The scope of the work

As discussed in the previous section many techniques employing both Optical-Xs both SAR multitemporal images have been developed principally to map and monitor fire scars. However, concerning the reforestation process, there is a lack on methodologies aiming at a quantitative estimation of vegetation's growing after fire. The few studies about this topic are limited in the near post fire (1-2 years after the fire) and give a qualitative idea of the process [31]-[34].

While optical and thermal sensors are sensitive to the initial changes in temperature and vegetative cover, SAR is sensitive to the longer-term moisture and roughness patterns that occur post-fire. This sensitivity of SAR makes it particularly useful for studying patterns of fire and variability in burn severity over long time spans. Moreover, SAR penetrates clouds and is characterized by the fact that when regeneration occurs after a fire, the enhanced backscatter may be shortened because the new vegetation may attenuate the signal.

The aim of this thesis work is to investigate the potentialities of multitemporal SAR data and electromagnetic models to derive some index significant for the monitoring of the recovery process inside a burned area, for a longer period than the near post fire. In particular, the work is focused on:

- a methodology to calculate a qualitative index of the reforestation process in burned area using multitemporal C band ERS-SAR data for a time of more than three years after the fire

- the use of "Water Cloud" model calibrated using some routines of the more sophisticated Tor Vergata scattering electromagnetic model for a quantitative retrieval of biomass growing rate (ton/ha per year).

The burned area chosen in this work to be monitored is the Castel Fusano pinewood, about 20 kilometres away from the main Rome urban centre (Italy). During the 3rd and 4th of July 2000, it was severely burned because of some fires that ruined about 350 ha of the wood: 250 ha were destroyed by the fire, while other 100 ha were seriously damaged.

Chapter 2 The Forward Problem

2.1 Introductive concepts

A vegetation canopy consists of a volume of scattering elements bounded by air on top and by a scattering soil surface at the bottom. The backscattering coefficient σ^0 is governed by the scattering properties of the vegetation elements and the soil surface, as well as by the interaction between the vegetation volume and soil surface in the form of multiple scattering. If the vegetation cover is sparse, as in some forested areas and during the early growth stages of some crops, the backscattering coefficient may be expressed in the form:

$$\sigma^0(\theta,\phi) = [1 - C(\theta,\phi)] \cdot \sigma^0_{bare} + C(\theta,\phi) \cdot \sigma^0_{can} + [1 - C(\theta,\phi)] \cdot \sigma^0_{\text{int}}(\theta,\phi) \quad \text{(2–1)}$$

where $C(\theta,\phi)$ is the fraction of the illuminated area that is vegetation-covered when observed along the direction (θ,ϕ), σ^0_{bare} is the backscattering coefficient of the exposed surface, σ^0_{can} is the backscattering coefficient of the canopy, which may include contributions from the vegetation cover and from the underlying surface, and σ^0_{int} is an interaction component accounting for multiple reflections (scattering) as in a corner reflector. These contributions are illustrated in Fig. 2.1. The multiple-reflection scattering component may in some cases be the dominant contributor because it depends on forward scattering by the canopy and the exposed surface, and if the exposed surface is smooth, as in the case of a water surface in a swamp with standing trees, the forward scattering component of the water surface may be several orders of magnitude larger than the backscattered component.

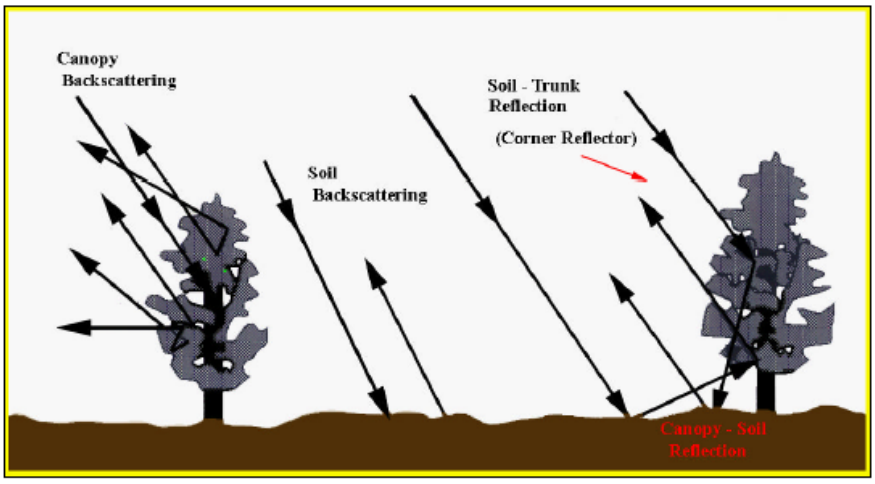

Fig. 2.1 The backscattered power may be composed of several contributions, depending upon the vegetation-cover fraction. The backscattered components may include direct backscattering from the exposed soil and vegetation, as well as multiply reflected forward scattering involving both the soil and the vegetation.

If the cover fraction approaches unity, σ^0 approaches σ^0_{can}. The modelling process involves two steps, the first relating the sensor output to the electromagnetic or model parameters of the scene and the second relating the model parameters to the physical parameters of the scene.

Considering a vegetation canopy as a lossy volume of scattering elements bounded above by air and below by a scattering soil surface, the model parameters include such factors as the scattering phase function, the extinction coefficient, and the scattering albedo, whereas the physical parameters include canopy geometry, canopy water distribution as a function of height and canopy constituents, and soil moisture content, among others.

Conceptually, given the model parameters for a vegetation canopy and the soil surface beneath it, the scattering coefficient $\sigma^0_{rt}(\theta)$, for any transmit-polarization configuration *t* and receive polarization *r*, can be computed. In practice some difficulties are encountered when modeling the backscattering behavior of a

vegetation canopy, specially in specifying model parameters that adequately describe the canopy. To develop an exact scattering model should be need:

- an exact description of the geometry, location, and dielectric properties of each element in the volume,
- models that describe the scattering behaviour of the individual elements,
- a model describing the scattering behaviour of the underlying soil surface.

For example, for a canopy consisting primarily of leaves, an appropriate scattering phase function may be developed when information is available about leaf-angle distribution, leaf-size distribution, and the dielectric properties of the leaf material. Furthermore the measure of these distributions for a given canopy is a time-consuming process and is seldom done in conjunction with remote-sensing observations.

Fortunately, the scattering process involves a certain amount of averaging as a result of the multiple scattering and the quasi-randomness of the locations, sizes, and orientations of the scatterers. This averaging effect, together with specific information about the attenuation properties of a given canopy constituent, often makes it possible to invoke approximations that simplify the scattering models into forms that are both easier to compute and more readily interpret-able in terms of the physical parameters of the scene. Hence, in modelling the scattering from vegetation, approximations are used, in part to simplify the problem, and in part to produce a model that applies to a class of vegetation canopies with similar geometries than to an individual crop type at a specified stage of growth. The leaves, for example, may be treated as circular or ellipsoidal discs[1] with an assumed distribution for their angular orientation, or the model may be simplified further by treating the leaves as isotropic scatterers. If the vegetation matter contained in a canopy volume is dominated by the leaves, or if the

[1] Leaves representation: for small leaves circular discs are appropriate; alternatives for long leaves planar elliptical discs; dielectric curved sheets (Sarabandi et al., 1988; Della Vecchia et al., 2004); subdivision into several circular discs (Fung, 1994; Bracaglia et al., 1995). Open problem: effects of ribs (and/or petioles) should be considered

leaves are large in size, the plant stalks often are ignored in modelling the scattering from such canopies. Large leaves behave like directional facets with strong reflections in the specular direction. If some of these leaves are oriented with their surface normals in the direction of the radar, they will exhibit a larger scattering coefficient than canopies with small leaves. If, on the other hand, the stalk[2] is considered to represent the major scattering model of the canopy, the scattering model may ignore the leaves and concentrate on the stalk.

2.2 The "Water Cloud" model

A simple approach to modeling the backscattering from vegetation canopy was proposed by Attema and Ulaby (1978) [36]. The vegetation volume is assumed to consist of identical scatterers that are uniformly distributed throughout the volume, as illustrated in Fig. 2.2

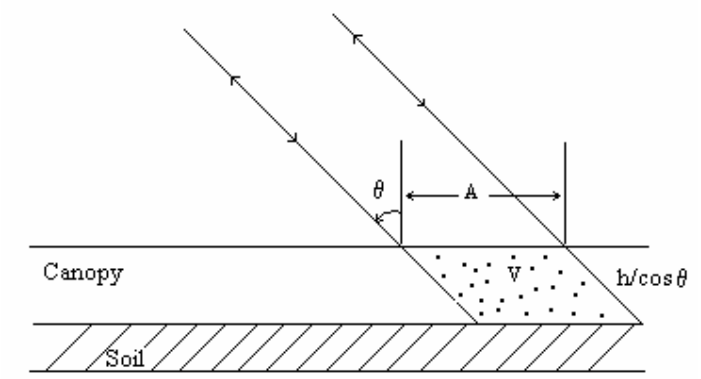

Fig. 2.2 Vegetation canopy modelled as a collection of ramdomly distributed scatterers

Ignoring multiple scattering, the volume backscattering coefficient σ_v (m^2m^{-3}) and the extinction coefficient k_e (m^{-1}) of the vegetation medium are given by:

[2] Stems representation : unique dielectric cylinder (general approach); subdivided into sections (Chiu and Sarabandi, 2000); subdivided into short dipoles (Stiles and Sarabandi, 2000); Hollow cylinder (DellaVecchia et al., 2004). Ears representation: simply neglected in some models, represented as dielectric cylinders; open problem: the ear is partially empty

(2–2) $\sigma_v = N\sigma_b$ (m^{-1}),

(2–3) $k_e = NQ_e$ (m^{-1}),

where N (m^{-3}) is the number of scattering particles per unit volume and σ_b (m^2) and Q_e (m^2) are the backscattering cross-section for a single particle and extinction cross-section for a single particle, respectively. With reference to Fig. 2.2 for an incidence plane wave with power density S, the power incidence upon an illuminated area A is

(2–4) $P_i = SA\cos\vartheta$ (W)

Since a vegetation canopy does not have a distinct air-vegetation boundary, the power backscattered by the canopy is due solely to volume scattering. Following the standard practise used in radar meteorology to compute the backscattered power for clouds and rain, the power backscattered from the canopy is determined by integrating the power backscattered from each layer of thickness dz over the slant range $h = SA\cos\vartheta$, taking into account the two-way attenuation by the vegetation layer between the scattering layer and the canopy surface. Thus, the backscattered power P_r at a distance R from the canopy is given by

(2–5) $$P_r = \frac{SA}{4\pi R^2}\cos\vartheta\int_0^{h/\cos\vartheta}\sigma_v \exp(-2k_e z)dz$$

With P_i and P_r proportional respectively to the square of magnitude of incidence and scattered electric fields, the vegetation backscattering coefficient σ_v^0 (m^2m^{-2}) will be given by:

(2–6) $$\sigma_v^0(\vartheta) = \frac{4\pi R^2 P_r}{AP_i} = \frac{\sigma_v\cos\vartheta}{2k_e}\left[1-\exp(-2k_e h\sec\vartheta)\right] = \frac{\sigma_v\cos\vartheta}{2k_e}\left(1-\frac{1}{L^2(\vartheta)}\right)$$

where

(2–7) $$L(\vartheta) = \exp(k_e h\sec\vartheta)$$

is the one-way loss factor of the canopy. The expression given by (2–6) accounts for only the backscattering contributions of the canopy; it doesn't contain contributions from the underlying soil surface. Assuming that the soil backscattering contributions add incoherently to the vegetation contributions, the canopy backscattering coefficient may be expressed in the following form:

$$\text{(2–8)}\quad \sigma_{can}^{0}(\vartheta) = \sigma_{v}^{0}(\vartheta) + \frac{\sigma_{s}^{0}(\vartheta)}{L^{2}(\vartheta)} \quad (\mathrm{m^2 m^{-2}})$$

where the $L^{-2}(\vartheta)$ accounts for the two-way attenuation loss experienced by the wave due to propagation through the lossy vegetation layer. The above expression may be extended a step further by relating k_e, σ_v, and σ_s^0 to the physical parameters of the canopy and underlying soil media. The canopy is a mixture of air (typically > 99% by volume) and vegetation material. The dielectric properties of the vegetation material are governed principally by the vegetation moisture content, thus the scattering and absorption properties of the vegetation volume are strongly related to the volumetric water content of the canopy m_v ($\mathrm{kg \cdot m^{-3}}$), which is given by

$$\text{(2–9)}\quad m_v = (W_w - W_d)n / h \quad (\mathrm{kg \cdot m^{-3}}),$$

where n is the number of plants per unit of area, h is the plant height, and W_w and W_d are the wet the dry mass of one individual plant, respectively. In the model developed by Attema and Ulaby, it was proposed that the canopy volume be represented by a "cloud" of N water particles per unit volume with mass m_v. For an atmospheric cloud, the volume extinction coefficient is proportional to the cloud water content m_v. Assuming that a similar relation applies to the canopy "cloud", k_e may be expressed as

$$\text{(2–10)}\quad k_e = A_1 m_v,$$

where A_1 is a constant at a given frequency, and may be different for different canopy geometries because k_e is the sum of the volume absorption coefficient k_a and the

volume scattering coefficient k_s, and the latter may be a function of the shape and sizes of the real scattering elements (size, stalks, and fruit). If the assumption that the scattering particles (representing the true scattering elements) are all identical in shape and sizes is reasonable, then, from (2–2) and (2–3) results that

(2–11) $$\frac{\sigma_v}{2k_e} = \frac{\sigma_b}{2Q_e}$$

which pertains to an individual particle and therefore is independent of m_v. Hence, at a given microwave frequency, $\sigma_v / 2k_e$ may be set equal to a constant B_1,

(2–12) $$\frac{\sigma_v}{2k_e} = B_1$$ (identical particles).

If, on the other hand, one were to assume that these equivalent water particles are distributed in size in a manner similar to the distribution of water spheres in an atmospheric cloud, the volume backscattering coefficient σ_v would be proportional to m_v^2; therefore,

(2–13) $$\frac{\sigma_v}{2k_e} = B_2 m_v$$ (particles distributed in size),

where B_2 is a constant at a given frequency and for a given canopy geometry.
Finally, the soil backscattering coefficient could be expressed in the following form,

(2–14) $$\sigma_s^0(\vartheta) = C(\vartheta)\exp(Dm_s)$$ ($m^2 \cdot m^{-2}$),

where $C(\vartheta)$ accounts for the dependence on the soil surface roughness and D is a constant coefficient representing the sensitivity of σ_s^0 to the soil moisture content m_s .Inserting (2–10) through (2–14) into(2–6) leads to

(2–15) $\sigma^0_{can}(\vartheta) = B_1 \cos\vartheta\left(1 - \frac{1}{L^2(\vartheta)}\right) + \frac{C(\vartheta)}{L^2(\vartheta)}\exp(Dm_s)$ for identical particles

and

(2–16) $\sigma^0_{can}(\vartheta) = B_2 m_v \cos\vartheta\left(1 - \frac{1}{L^2(\vartheta)}\right) + \frac{C(\vartheta)}{L^2(\vartheta)}\exp(Dm_s)$

for particles distributed in size.

For a given canopy, the loss factor $L(\vartheta) = \exp(A_1 m_v h \sec\vartheta)$ increases with:

1. increasing angle of incidence ϑ due to the enhance in slant height, $h\sec\vartheta$
2. increasing volumetric water content m_v
3. increasing microwave frequency through the coefficient A_1.

Thus, if the frequency is sufficiently low and/or the angle of incidence is close to nadir, the canopy behaves like a low-loss dielectric layer with a loss factor $L(\vartheta)$ close to unity, in which case $\sigma^0_{can}(\vartheta)$ reduces from (2–15) and (2–16)to

(2–17) $\sigma^0_{can}(\vartheta) \cong \sigma^0_s(\vartheta)$ (if $L(\vartheta) \approx 1$).

The opposite limiting case is that corresponding to a very lossy canopy whose L is sufficiently large that $1/L^2(\vartheta)$ could be neglected in the first term in (2–15) and (2–16), and also the soil term could be neglected in comparison with the first term. For this case the (2–15) and (2–16) reduces to

(2–18) $\sigma^0_{can}(\vartheta) = B_1 \cos\vartheta$ for identical particles and

(2–19) $\sigma^0_{can}(\vartheta) = B_2 m_v \cos\vartheta$ for particles distributed in size.

Anyway for the general case, the behaviour of the canopy to be described needs the fully expression given by (2–15). Even if the combination of observation angle ϑ and frequency f is such that the soil contribution is negligible during the fully grown and green stages of a canopy, the soil contribution have to be included during the early

stage of growth if a significant portion of the soil is exposed, and during the stage prior to harvest for many types of crops, because the plants lost of their water content during this stage. Attema and Ulaby (1978) tested the applicability of model described using measured data acquired at several frequencies between 8 and 18 GHz over the 0-70° angular range. The data were acquired for fields of alfalfa, corn, milo and wheat, as a function of time over the growing season with, with a spacing between measurements of about one to weeks. The parameters m_v, h, m_s were measured in conjunction with each radar observations. Using regression analyses, they determined the values of constants A_1, B_1, C, D, for each crop type, polarization configuration and microwave frequency by fitting the measured data with (2–15).

Then they evaluated the model by comparing the measured with predicted temporal record of σ^0. Examples are shown in Fig. 2.3 for incidence angle range from 0° to 50°, for corn and alfalfa. The model was further evaluated comparing the measured values of σ^0 of all data sets over the observation period (for a given crop type) for the full 0-70° angular range and Fig. 2.4 shows the results for the VV polarization at 17 GHz. The linear correlation coefficient ρ between measured and predicted values of σ^0 ranged between 0.74 and 0.98 for alfalfa. Although this simple cloud model appears to provide an adequate description of overall behaviour of σ^0_{can} as function of angle ϑ and of three canopy and soil parameters (m_v, h, m_s), it is by no means an exact or perfect model, it should be regarded as a general first-order model.

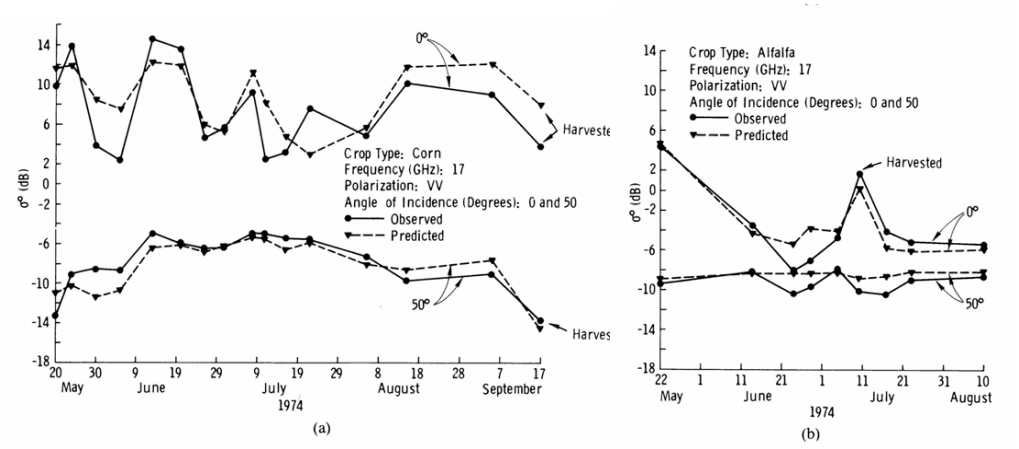

Fig. 2.3 Observed and predicted temporal responses of σ^0 for (a) corn, (b) alfalfa at 17 GHz (Attema and Ulaby 1978)

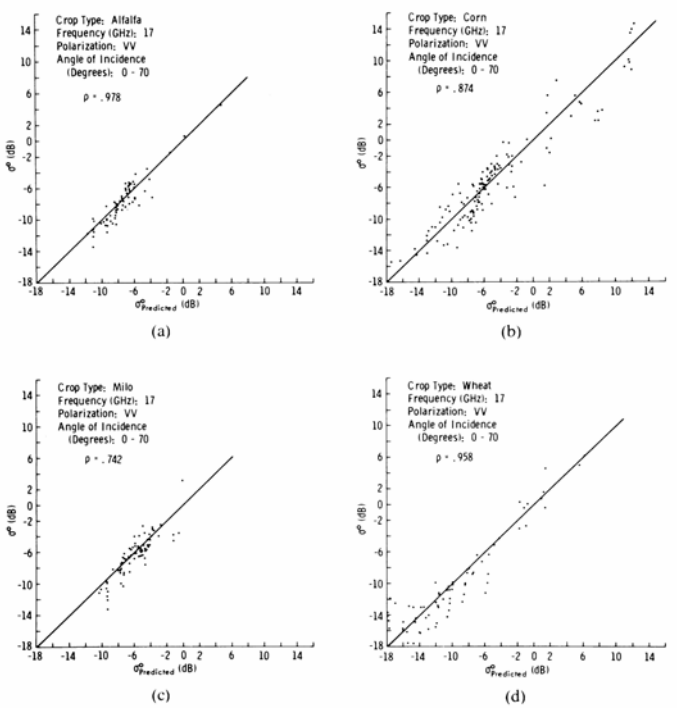

Fig. 2.4 Measured versus predicted values of σ^0 for four crops at 17 GHz: (a) alfalfa, (b) corn, (c) milo, (d) wheat.

The major limitation of the cloud model is that it doesn't take into account in any direct way for the geometry of the scattering elements in the canopy; rather, these geometrical factors are accounted for empirically through the constants A_1 and B_1 or B_2. If all the canopies have the same scattering and absorption behaviour as a function of m_v, the value of A_1 would have to be the same for all four crop types at a given frequency. As a result of fitting the observed data to the model equation, Attema and Ulaby (1978) found that at a given frequency *f*, the magnitude of A_1 is about two orders of magnitude larger for alfalfa than for corn.

Because each of these values was derived from fits using data acquired over the full observation period, which included more than one major stage of growth, it represents an average or effective value of the attenuation properties of that crop. To take into account the geometrical changes that a crop canopy undergoes as it progresses from one stage of growth to another, a more sophisticated model than a cloud model is needed. Additionally, as formulated, the cloud model treats the entire canopy as having uniform characteristics over its height *h*, which usually is not the case, particularly for tree canopies.

2.2.a A more compact expression for the model

If the dependence of physical parameters is required, remembering that $L(\vartheta) = \exp(k_e h \sec\vartheta)$ and $k_e = A_1 m_v$ the (2–15) becomes

$$\sigma^0_{can}(\vartheta) = B_1 \cos\vartheta\left(1 - \exp(-2A_1 m_v h \sec\vartheta)\right) + \sigma^0_s(\vartheta)\exp(-2A_1 m_v h \sec\vartheta) \quad (2\text{–}20)$$

where $\sigma^0_s(\vartheta) = C(\vartheta)\exp(Dm_s)$.

If the following positions have been supposed

$$w = m_v h \quad (\text{kg/m}^2), \quad (2\text{–}21)$$

that is the water content of the canopy per m^2,

(2–22) $d = 2A_1 \sec\vartheta$ (m^2/kg),

(2–23) $c = B_1 \cos\vartheta$,

the expression of $\sigma^0_{can}(\vartheta)$ will be reduced in the simple following form

(2–24) $\sigma^0_{can}(\vartheta) = c(1 - \exp(-d \cdot w)) + \sigma^0_s \exp(-d \cdot w)$

At last expressing the product $(d \cdot w)$ as

(2–25) $\tau = d \cdot w$

the expression of $\sigma^0_{can}(\vartheta)$ will become again more compact

(2–26) $\sigma^0_{can}(\vartheta) = c(1 - \exp(-\tau)) + \sigma^0_s \exp(-\tau)$

2.3 Integration of the "Water Cloud" model with the "Tor Vergata" discrete element model

As assumed in the previous paragraph, the values of constants A_1, B_1, C, D of the model are calculated using regression analysis fitting the measured data m_v, h, m_s in conjunction with each radar observation. In the present work, considering the expression (2–24) of $\sigma^0_{can}(\vartheta)$, that is reported below for simplicity,

(2–24) $\sigma^0_{can}(\vartheta) = c(1 - \exp(-d \cdot w)) + \sigma^0_s \exp(-d \cdot w)$

the coefficients ***c*** and ***d*** have been calculated using some routines of the "Tor Vergata" discrete element scattering model [37], that is, as previously said, a more complicated model than the "Water Cloud" one. A brief review on the Tor Vergata model is reported in the following section. Anyway, for all the considerations concerning the hypothesis assumed to calibrate the Water Cloud model with the Tor Vergata Model and to retrieve the biomass value see the chapter 5.

2.4 The "Tor Vergata" scattering model

The scattering model developed at Tor Vergata University [38] is based on the Radiative Transfer theory and describes vegetation as a homogeneous half space overlayed by an ensemble of discrete dielectric scatterers[3]. The single scatterer behaviour is described by the complete bistatic scattering cross-section. The contributions of the various scatterers are combined by means of a numerical algorithm named Matrix Doubling [39], [40]. This model offers the following advantages:

- Multiple scattering effects of any order are included;
- The whole microwave spectrum is covered;
- Both backscatter coefficient and emissivity (for passive systems) may be computed.

In particular, the model developed describes the medium as sketched in Fig. 2.5

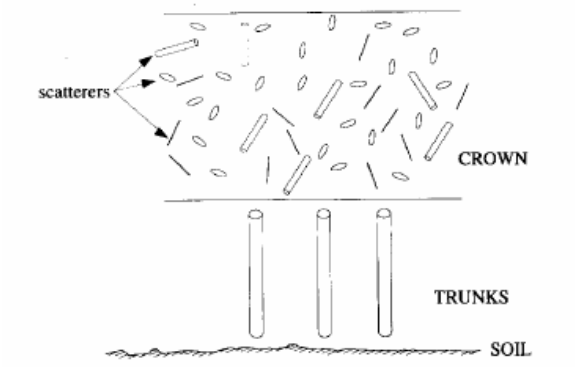

Fig. 2.5 Draft representation to model the medium

[3] *Stems representation* : unique dielectric cylinder (general approach); Hollow cylinder (DellaVecchia et al., 2004). *Leaves representation*: for small leaves (alfalfa, soybeans) circular discs are appropriate; alternatives for long leaves (corn, wheat) planar elliptical discs (overestimate directivity); dielectric curved sheets (Della Vecchia et al)

The medium is subdivided into three main regions: crown, trunks, soil. The crown is filled with scatterers representing leaves, needles, twigs and branches. They may be positioned at various heights, according to the properties of the tree species to be modelled. The scatterers of different kinds are uniformly located within the crown. For discs (deciduous leaves) and needles (coniferous leaves) the Rayleigh-Gans approximation [41] is used at P, L and C band.

According to this theory, the inner field of an object with at least one dimension small with respect to the wavelength can be approximated with a homogeneous field along this dimension, while in the other two dimensions phase differences must be taken into account. Also the Physical Optics approximation [42], which substitutes the field inside a thin disc with the one of a slab with the same thickness, has been implemented to compute disc electromagnetic properties at higher frequencies. The infinite length approximation[43], which approximates the field inside a finite cylinder with that of an infinite one, is used for cylindrical objects like twigs, branches and trunks.

This formulation of the scattering function is based on a lengthy algorithm which requires much computer time, due to the complex representation of the permittivity, and to the infinite expansion in Bessel and Hankel functions. In the implementation of the Tor Vergata model this problem has been overcome by calculating automatically the maximum number of Bessel and Hankel functions (which on its turn increases with the cylinder dimensions relative to frequency) necessary to reach the convergence of the results; on the other hand, for large (with respect to wavelength) cylinders it has taken advantage of the increasing scattering directivity.

An important parameter which controls scattering from vegetation is the dielectric constant. It has been computed through the semi-empirical formula, given in [44], which needs the moisture content and the wet to dry density ratio as inputs. The soil is described as a homogeneous half-space. Out of the several theories proposed for soil scattering, in the model is applied the Small Perturbation approximation. The soil permittivity is computed according to the semiempirical formula proposed

in [45]. By using the above mentioned approximations, the amplitude scattering functions

$$\begin{matrix} f_{vv}(\theta,\phi,\theta_s,\phi_s) & f_{vh}(\theta,\phi,\theta_s,\phi_s) \\ f_{hv}(\theta,\phi,\theta_s,\phi_s) & f_{hh}(\theta,\phi,\theta_s,\phi_s) \end{matrix} \quad (2\text{–}27)$$

of individual crown scatterers are computed for the assumed Eulerian angles α, β, γ.

θ and θ_s denote incidence and scattering off-normal angles, respectively, while ϕ and ϕ_s denote incidence and scattering azimuth angles. The bistatic scattering cross-sections $\sigma_{pq}(\theta,\phi,\vartheta_s,\phi_s) = 4\pi\left\langle f_{pq}^2(\theta,\phi,\vartheta_s,\phi_s)\right\rangle$ are then obtained averaged over the assumed range of Eulerian angles; p and q denote polarizations of scattered and incident fields, respectively.

The extinction cross-sections $\sigma_{eq}(\theta,\phi)$ of individual crown scatterers are also computed; to this aim, the forward scattering theorem is used for the case of cylinders, while the sum of absorption and scattering cross-sections is taken for the case of discs. The following functions are also computed: trunk bistatic scattering cross-section in the specular direction $\sigma_{tqq}(\theta,\phi,\theta_s=\theta,\phi_s=\phi+\pi)$, trunk extinction cross-section $\sigma_{teq}(\theta,\phi)$, soil bistatic scattering coefficient $\sigma_{gpq}(\theta,\phi,\theta_s,\phi_s)$.

Once the above indicated quantities are known, the different contributions are combined by means of the Matrix Doubling algorithm and the overall backscatter coefficient is obtained.

Other medium parameters, like soil moisture, soil roughness standard deviation, trunk moisture, branch moisture, leaf moisture and dimensions, are assumed to be constant and their values are deduced on average by data available in the literature. Computations could be carried out at VV, HV and HH polarizations and using different incidence angles θ.

2.4.a Hypothesis on canopy structure

Relating to that a given amount of crown woody matter could be either concentrated in few large branches or distributed in many small branchlets, the hypothesis relating to the canopy structure are carried out at single-scatterer level and canopy level.

In the first case, dielectric cylindrical scatterers are considered, whose properties represent, on average, those of some "realistic" branches. The following parameters are assumed: the incidence angle θ, the *c*ylinder radius (a_B), the cylinder length (l_B = N a_B), the moisture content (m_B = % by weight). The orientation is random, i.e., the cross-sections are averaged over Eulerian angles α, β, γ with $0< \alpha < 360^o$, p(α)=1, $0<\beta < 90^o$, p(β)=1, $\gamma = 0^o$.

With reference to canopy analysis, canopies uniformly filled with equal cylinders are considered. The parameters are the same of the previous analysis and obviously the total volume is considered. To keep the total volume constant when the single cylinder volume is increased, the cylinder density is assumed to be inversely proportional to the single cylinder volume itself.

For a given overall branch volume, the backscatter coefficient may show significant variations depending on the dimensions and orientation of the cylindrical elements filling that volume. It follows that direct or inverse algorithms relating σ^0 to the woody volume (or to the biomass) cannot be independent on the tree species, but must be tailored to the particular morphological characteristics of the species under consideration.

Chapter 3 The Castel Fusano pinewood fire event: the data set

3.1 Introduction: study area

This work considers the very dramatic fire event which occurred in the Castel Fusano pinewood, located few kilometers away from Rome main urban area, on July 2000. The Castel Fusano pinewood belongs to “Riserva Naturale Statale Litorale Romano”, a state natural reserve of the roman coast, which covers a region of about 15900 ha placed around the delta of the River Tevere, about 20 kilometres away from the main Rome urban centre (Fig. 3.1).

The reserve is characterized by the presence of different types of surroundings, typical of the coastal area of the Mediterranean: oaks and pines dominate the arboreal vegetation, with large part of the Park covered by the tall evergreen Mediterranean bush.

The Castel Fusano Park is located in the south part, five kilometres from the delta, and extends over an area of approximately 1,100 ha; its main land cover types are Quercus ilex L., Phillyrea latifoglia L., Pistacia lentiscus L. and anthropic Pinus pinea L. plantations introduced by the coast starting from 18th century; actually inside the park, cohabit “the old pinewood” with an age of 130-150 years and “the young woodland” that is 50-60 years old.

Until the 3rd of July, 2000, the pinewood was only slightly damaged by not particularly serious frequent fires. Nevertheless on 3rd and 4th of July 2000, the pinewood went severely burned because of some fires that ruined about 350 ha of the wood and about 250 ha of wood were destroyed by the fire, while other 100 ha were seriously damaged. Particularly devastating was the 4th of July fire, which

had more than one fire point in the South-West part of the pinewood, where it borders the Castelporziano Presidential Estate (Fig. 3.2).

Fig. 3.1 Image acquired on 23/09/1999 by Landsat 5 satellite

Soon after the fire, Municipality of Rome has decided a plan for the reclamation of the area and for restoring the local ecosystem.

In the manner provided for by the plan some main actions consist in the cutting and removal of vegetation irremediably damaged, in the singling out the trees for which spontaneous recovery was still possible, in the replantation of the main cover types of pinewood, principally Pinus pinea L. and Quercus ilex L. plantations.
Moreover, experimental areas particularly dedicated to the monitoring of the only spontaneous processes have been identified.

Fig. 3.2 On the left side a photograph of the pinewood before the fire event; on the right side a pinewood area after the fire

3.2 The dataset

The dataset used consists of images acquired by different platform and sensors and consists of:

- georeferenced aerial ortophotos, 1m of resolution, used to reconstruct the scenario before the fire event.

- airborne images, about 1m resolution, acquired in the visible and near infrared band range immediately after the fire (18-21 July 2000) by Municipality of Rome

- one Landsat 5 TM imagery, taken on 25/09/2000.

- time series of descending ERS-SLCI (Single Look Complex full frame) SAR images

A significant set of ERS-SAR images has been collected before and after the fire event consisting in an overall number of 34 satellite passes. Reminding that the fire event occurred on 4 July 2000, the considered time window goes from February 1999 to October 2003 so it comprises more one year before the fire event and three years after.

For each pass, investigation on meteorological condition has been carried out [46]; these latter are indicated in the rightmost two columns of Table 1 where the complete list of the considered SAR images is reported.

3.3 The methodology

A ground range backscatter intensity time series of ERS-SAR images has been carried out by developing and optimising of a procedure that performs an automatic coregistration, a conversion from slant range to ground range geometry and the calibration process; then an average in azimuth has been implemented to achieve a regular pixel size (17m) and a reduction of speckle (in Fig. 3.3 the process flow is described).

Concerning the airborne images after the fire, a mosaic covered all the Castel Fusano pinewood has been realized. Finally a registration on the georeferenced orthophoto, with an RMSe less than one pixel, has been performed, making all the data georeferenced and overlapped, integrated in a G.I.S.

Date	Days from event fire	Satellite	Orbit	Passage	Frame	Track	Weather cond.	UP
14 Feb. 1999	-540	ERS-2	19973	D	2763	79	Clear	2
21 March 1999	-505	ERS-2	20474	D	2763	79	Clear	-
25 April 1999	-470	ERS-2	20975	D	2763	79	Scattered Clouds	1
30 May 1999	-435	ERS-2	21476	D	2763	79	Clear	-
4 Jul. 1999	-366	ERS-2	21977	D	2763	79	Clear	-
08 Aug 1999	-331	ERS-2	43153	D	2763	79	Clear	-
12 Sep 1999	-296	ERS-2	22979	D	2763	79	Clear	5
17 Oct. 1999	-261	ERS-2	23480	D	2763	79	Partly Cloudy	1
21 Nov. 1999	-226	ERS-1	23981	D	2763	79	Thunderstorm	0
29 Jan. 2000	-156	ERS-1	44656	D	2763	79	Mostly Cloudy	0
14 May 2000	-51	ERS-2	26486	D	2763	79	Clear	5
18 Jun. 2000	-16	ERS-2	26987	D	2763	79	Partly Cloudy	2
7 Jul. 2000	+3	ERS-2	27259	D	2763	351	Clear	-
1 Oct. 2000	+89	ERS-2	28490	D	2763	79	Partly Cloudy	0
5 Nov.2000	+124	ERS-2	28991	D	2763	79	Scattered Clouds	2
10 Dec. 2000	+159	ERS-2	29492	D	2763	79	Partly Cloudy	-
14 Jan. 2001	+194	ERS-2	29993	D	2763	79	Scattered Clouds	5
18 Feb. 2001	+229	ERS-2	30494	D	2763	79	Partly Cloudy	-
03 June 2001	-334	ERS-2	31997	D	2763	79	Scattered Clouds	-
8 Jul. 2001	+369	ERS-2	32498	D	2763	79	Scattered Clouds	-
12 Aug2001	+434	ERS-2	32999	D	2763	79	Clear	-
16 Sep. 2001	+439	ERS-2	33500	D	2763	79	Mostly Cloudy	1
21 Oct 2001	+474	ERS-2	34001	D	2763	79	Clear	-
25 Nov. 2001	+509	ERS-2	34502	D	2763	79	Clear	6
14 Apr. 2002	+649	ERS-2	36506	D	2763	79	Light Rain	0
23 Jun. 2002	+719	ERS-2	37508	D	2763	79	Clear	-
28 Jul. 2002	+754	ERS-2	38009	D	2763	79	Clear	-
1 Sep. 2002	+789	ERS-2	38510	D	2763	79	Mostly Cloudy	1
10 Nov. 2002	+859	ERS-2	39512	D	2763	79	Partly Cloudy	2
19 Jan. 2003	+929	ERS-2	40514	D	2763	79	Clear	1
30 Mar. 2003	+999	ERS-2	41516	D	2763	79	Clear	-
8 Jun. 2003	+1069	ERS-2	42518	D	2763	79	Scattered Clouds	-
17 Aug. 2003	+1139	ERS-2	43520	D	2763	79	Clear	-
26 Oct. 2003	+1209	ERS-2	44522	D	2763	79	Clear	3

Table 1 List of the SAR images considered for the study. The UP column shows the number of days occurring between the last rainy day and the day of the measurement (0 means rain in the date of acquisition; - means that such number was greater than 7).

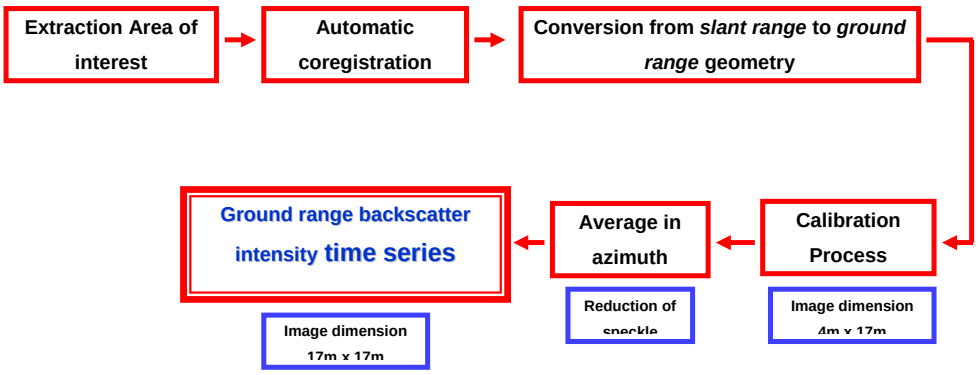

Fig. 3.3 Procedure flow developed to carried out the ground range backscatter intensity time series of ERS-SAR images

By using the high resolution aerial photographs and images before and after the fire event, the historical fire archives and the actual time plan of intervention on fire-affected region, 14 different regions of interest (ROI), described in detail in Table 2, have been selected and recorded in a vector layer employed for the classification and segmentation of the SAR images.

These 14 ROIs were regrouped into the following 3 greater thematic classes.

- A class made up of regions destroyed by the fire where the process started or by artificial interventions of reclaiming and plantation or completely spontaneous with no man-made actions. This class, that has been called "**Burned area**" (***Ba***), includes the **ab1, ab2, ALotto2, AS, AT, APG, ATP** and **A77-00** with a total surface extension of 26,2 ha; in Fig. 3.4 is reported the time behaviour of backscattering coefficient for each area.

- A class made up of young and old pinewood and a mediterranean scrub vegetation area which was not damaged by the fire event, that has been called "**Not Burned area**" (***NBa***) and includes the **AC**, **APGc** and **A77** ROIs with a total surface extension of 17,4 ha; in Fig. 3.5 is reported the time behaviour of backscattering coefficient for each area.

	AREA name (ha)	Description of area
1	**ab1** (4.9 ha)	An old pinewood area destroyed by the fire of 2000, that underwent artificial interventions of reclaiming from January 2001 to June 2001 and plantation with very young plants (1m height) starting to January 2003.
2	**ab2** (2.9 ha)	An old pinewood area destroyed by the fire of 2000, which underwent artificial interventions of reclaiming from June 2001 to March 2003 and plantation with young plants (1m height) starting to January 2003.
3	**ALotto2** (6.7 ha)	An old and young pinewood area destroyed by the fire of 2000, which underwent artificial interventions of reclaiming from March 2001 to June 2001 and contemporary plantation with young plants (4m height).
4	**AS** (4.3 ha)	A old pinewood area destroyed by the fire of 2000, which underwent artificial interventions of only reclaiming from late months of 2002 to March 2003
5	**AT** (3.1 ha)	A old pinewood region destroyed by the fire of 2000, where the process has been completely spontaneous with no man-made actions
6	**APG** (1.4 ha)	A young woodland area destroyed by the fire of 2000. The process was spontaneous.
7	**ATP** (1.9 ha)	Young woodland region that suffered the fire of 1984 and of 2000. After the first fire the process was spontaneous and when the 2000 fire happened the area was populated by overall Mediterranean scrub vegetation. Also after 2000 fire the has been spontaneous.
8	**A77-00** (2.9 ha)	A mediterranean scrub vegetation area that suffered a fire of 1977 and that of 2000. Both the fire of 1977, both after the fire of 2000, the process has been spontaneous.
9	**AC** (9.4 ha)	An old pinewood area not burned by the fire
10	**APGc** (3.8 ha)	A young pinewood area not burned by the fire
11	**A77** (4.2 ha)	A mediterranean scrub vegetation area that suffered a fire 1977. After the fire, the process has been spontaneous.
12	**VCNord** (3.9 ha)	An area that suffered two fires (1977 and 1984) before the fire of 2000. When the fire of 2000 happened it was essentially a grass land area
13	**AGariga** (1.5 ha)	Very frequently burned, this area is fundamentally a grass land area
14	**NoVegetation** (14.8 ha)	A region inside the close area of Castel Porziano consisting of soil characterized by almost absence of vegetation

Table 2 Details of 14 Region of interest selected in the area under study. It's important to underlain that the interventions of reclaiming consist in thinning and burned biomass clearing.

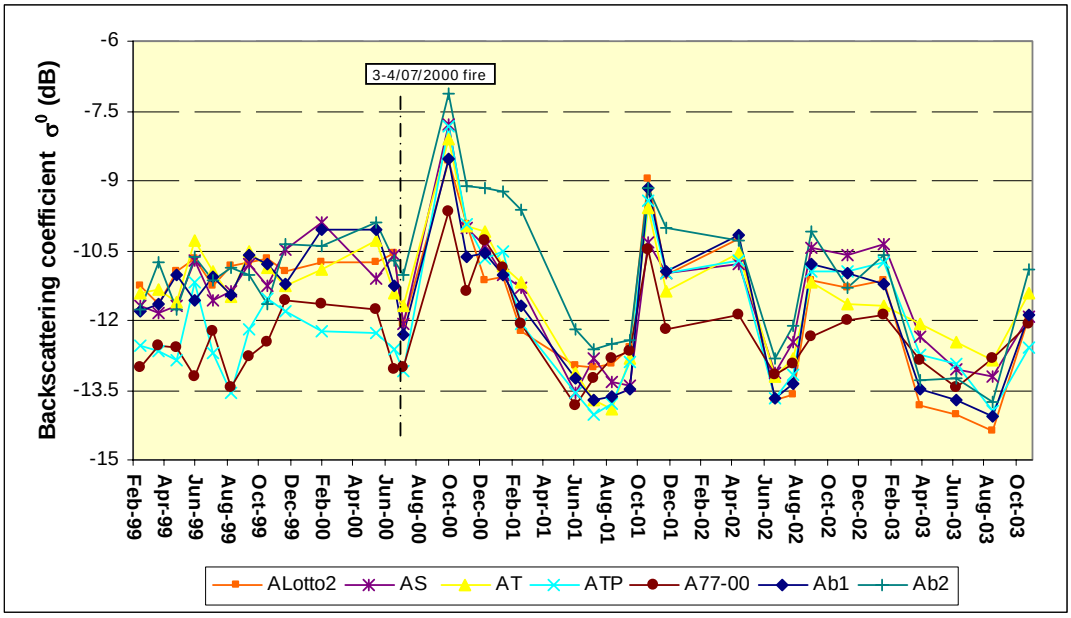

Fig. 3.4 Time behaviour of backscattering of ab1, ab2, ALotto2, AS, AT, APG, ATP areas

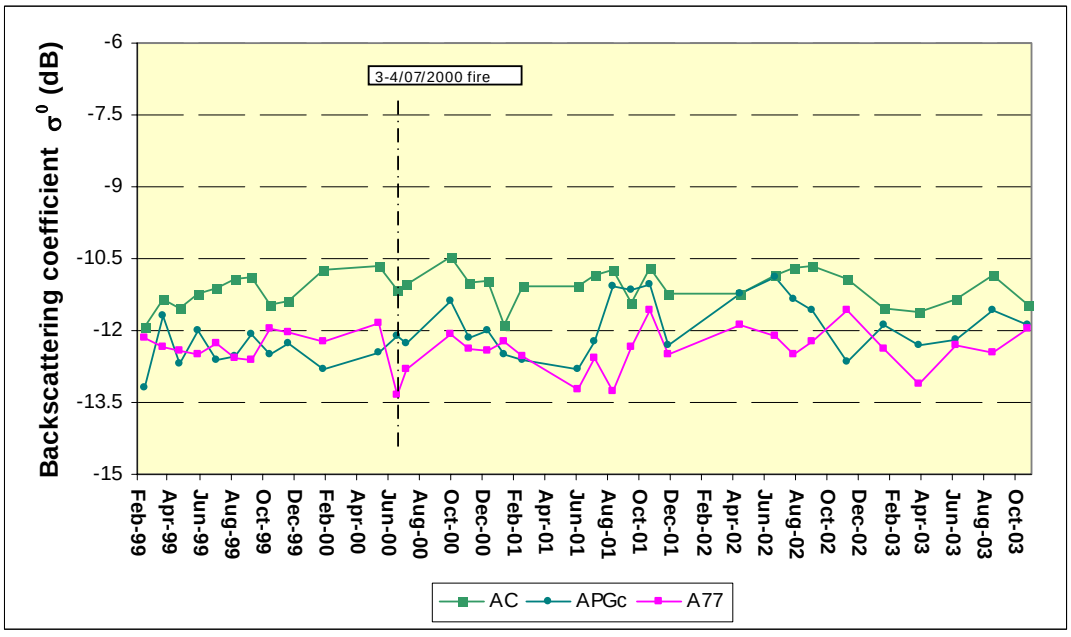

Fig. 3.5 Time behaviour of backscattering of AC, APGc, A77 areas

- A class basically consisting of soils characterized by absence of vegetation or rare grass vegetation, that has been called "**Bare Soil Like area**" (***BSLa***) and that includes the **VCNord**, **AGariga** and **NoVegetation** ROIs with a total surface extension of 20,2 ha; in Fig 3 is reported the time behaviour of backscattering coefficient for each area

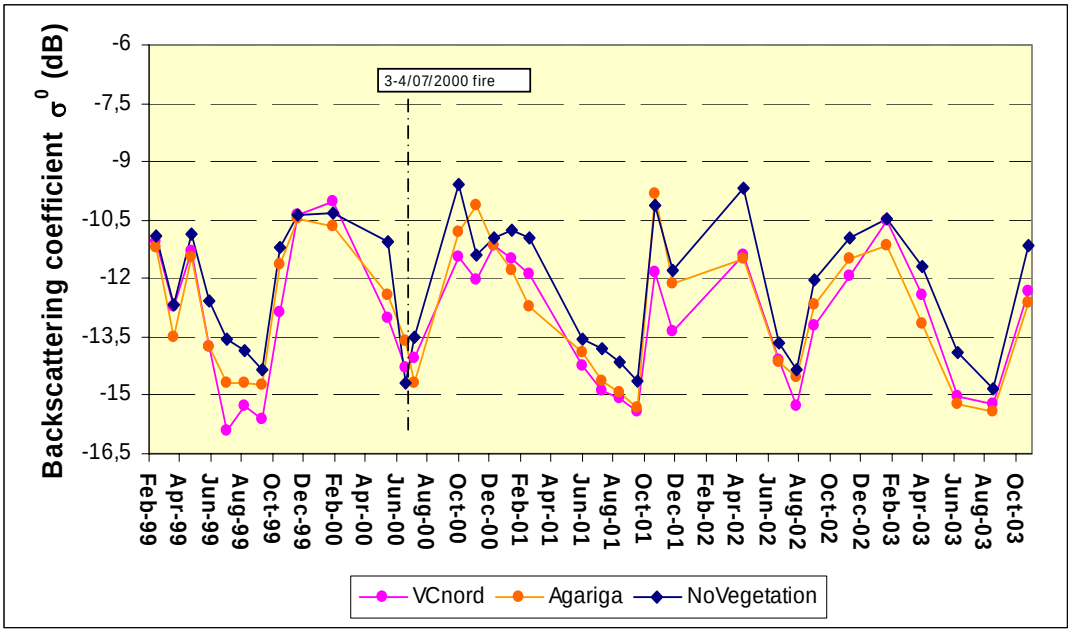

Fig. 3.6 Time behaviour of backscattering of VCNord, AGariga and NoVegetation areas

In particular, Fig. 3.7 shows the localization with different colours. of the classes described inside the area of Castel Fusano pinewood employing a post fire date SAR time series

From these trends it is evident the different behaviour of the three macro-regions *Ba*, *NBa* and *BSLa*. The *NBa* curves are enough stable and are comprised in a little range of variation, about 1.5 dB, without to be much affected from seasonal changes. On the other side, the *LBSa* curves have oscillating values, strongly connected to the seasonal periods of the year, with excursions of about 5-6 dB. In

this case, the soil moisture, driving the dielectric constant value of the soil, influences significantly the backscatter behaviour.

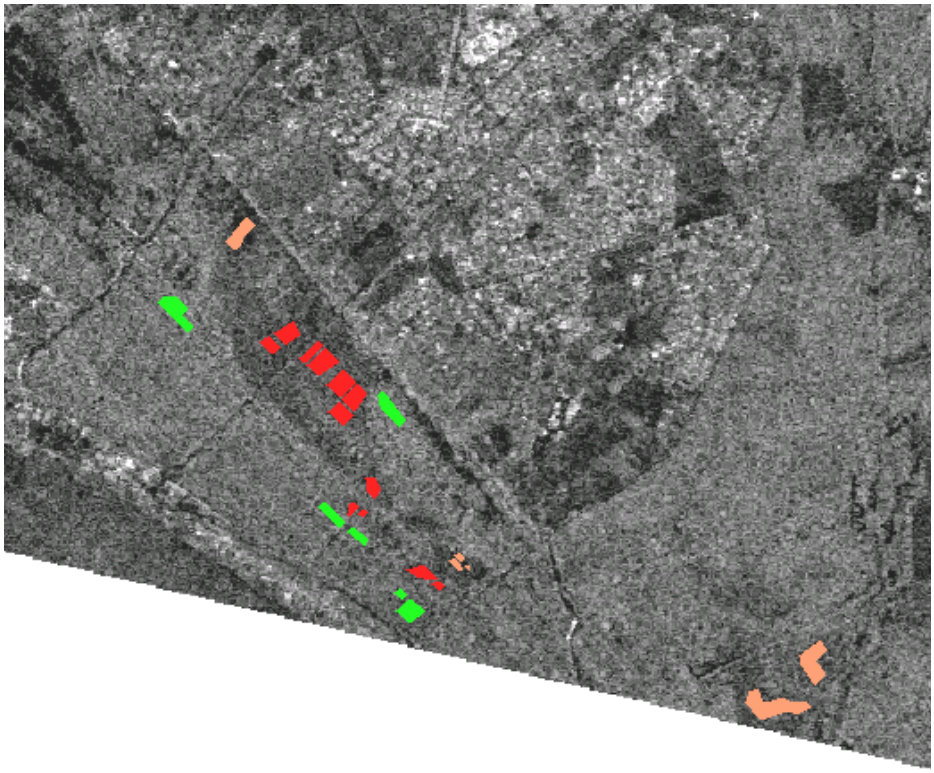

Fig. 3.7 The figure shows the localization (in a post fire SAR imagery) of the tree thematic classes identified with different colors: in red colour the “Burned area” (*Ba*), in green colour the “Not Burned area” (*NBa*), and in orange colour the “Bare Soil Like area” (*BSLa*).

Concerning the *Ba* curves, one can note that before the fire they have a behaviour quite similar to that of *NBa*, after the fire they begin to oscillate in the same way of of *BSLa* but reducing their dynamic range with the time.

As it will be explained in the next chapter, these behaviours are the starting point of the next analysis but it should be immediately noticed how multitemporal backscattering information content can be considered for a qualitative time monitoring of different target areas.

Chapter 4 Scar detection and multitemporal Analysis

4.1 The fire scar detection

An analysis, firstly, on the capability of detecting fire scars with SAR data has been carried out, considering a TM Landsat 5 image (taken on 25/9/2000) as ground truth. Indeed, Fig. 4.1 shows how the scar is easily detectable by using Landsat 7, 4 and 3 bands.

Fig. 4.1 TM Landsat image (bands 7, 4, 3) taken on 25 September 2000: the fire scar is in brown colour.

By chance, the first ERS pass after the fire event was very early, on 2000 July the 7th, but though a general lower value of backscattering can be visible in the burned area (about 0.5 db respect to the area not burned), this is not clearly discernible in the SAR image which is reported in Fig. 4.2.

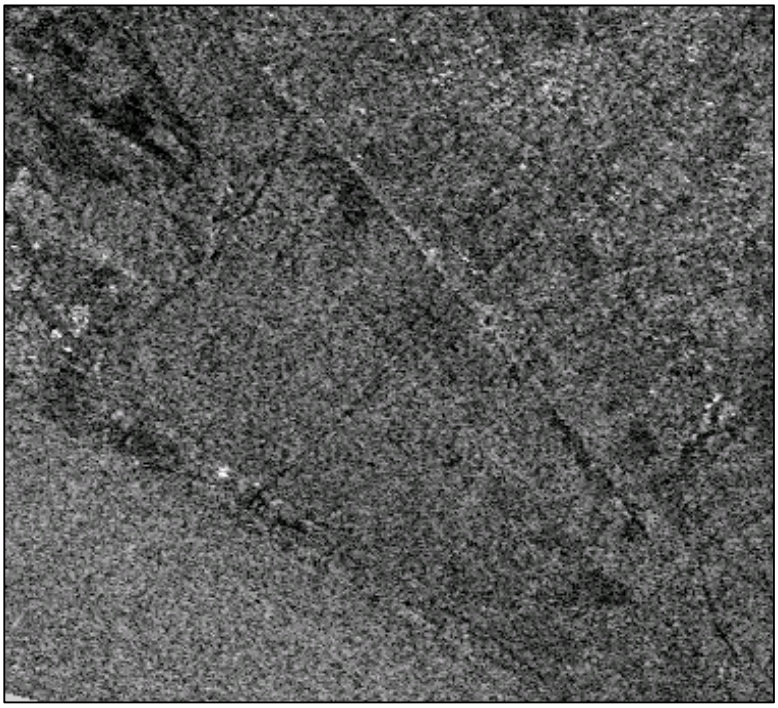

Fig. 4.2 ERS SAR image taken on 7 July 2000

For sake of comparison, in Fig. 4.3(a), a SAR image obtained by averaging all the available passes preceding the event is also shown.

The lower value of the backscattering should be given to the fact that the return is dominated by the soil contribution. In summer season this is characterized by low values of moisture and, in turn, of backscattering. The same type of hypothesis may be considered to comment Fig. 4.3(b) and Fig. 4.3(c), given by averaging on two different sets of multitemporal images. Fig. 4.3(b) derives from the averaging of the first summertime (June, July, August, September of 2001 year) dates available after the fire event, on the other hand, Fig. 4.3(c) is the result of the average of the

autumn-winter time (January, February, October, November of 2001 year) images taken after the event. In both figures, we again can observe the significant effect of the soil moisture on the return corresponding to the burned area.

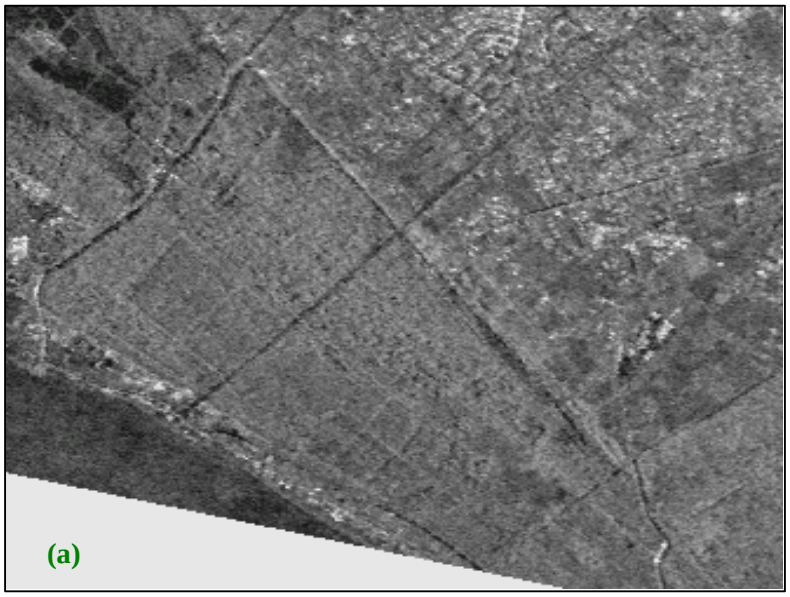

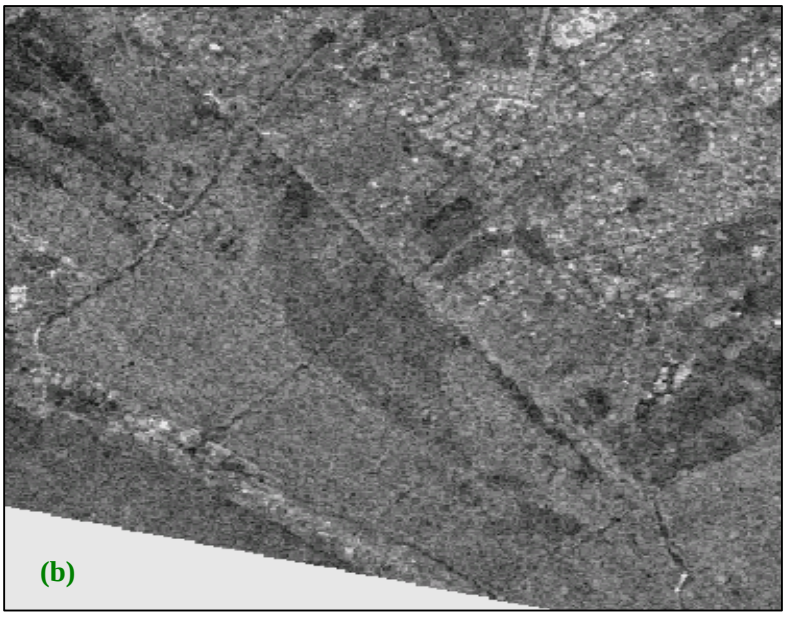

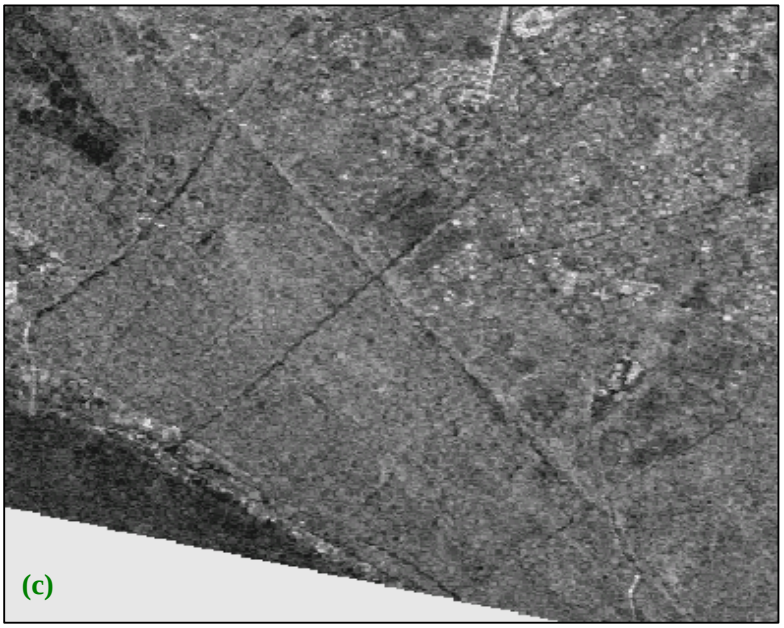

Fig. 4.3 (a) is an average SAR image obtained by averaging all the available passes in 1999; (b) is the average SAR image considering the first summertime (June, July, August, September 2001) dates available after the fire event and (c) is the average SAR image considering the autumn-winter time acquisitions (January, February, October, November 2001).

In summertime soil moisture values are lower and, as seen before for a single image, this provokes a lower value of the backscattering (about 2 dB) with the respect to the surrounding not-burned area, where the volume scattering of the trees dominates. The behaviour is opposite during wintertime, when a higher soil moisture makes the backscattering of the pixels corresponding to the fire scar higher (more than 1dB) than that of those belonging to the surrounding areas.

Hence, it's clear that with only one SAR image it's not easy to define the fire scars and considering absence of clouds the single optical image would be much more effective to the specific purpose. Nevertheless, if after the fire a set of images, acquired in the same season, is available, it is possible to achieve good level of accuracy for the discrimination of burned regions.

4.2 The "re-growing" process monitoring

As seen in section 3.3, the influence of the soil moisture on the backscattering seems to be significant also for understanding how the process may be monitored by multitemporal measurements.

In fact, as the reforestation goes on in the burned area, the corresponding backscattering tends to be less affected by the surface scattering effects typical of the soil, becoming more similar to the volume scattering typical of the parts of the pinewood not affected by the fire.

This can be noted in Fig. 4.4 where are plotted the backscattering coefficient trends relatively to the three main areas of interest *Ba*, *NBa* ans *BSLa* described before.

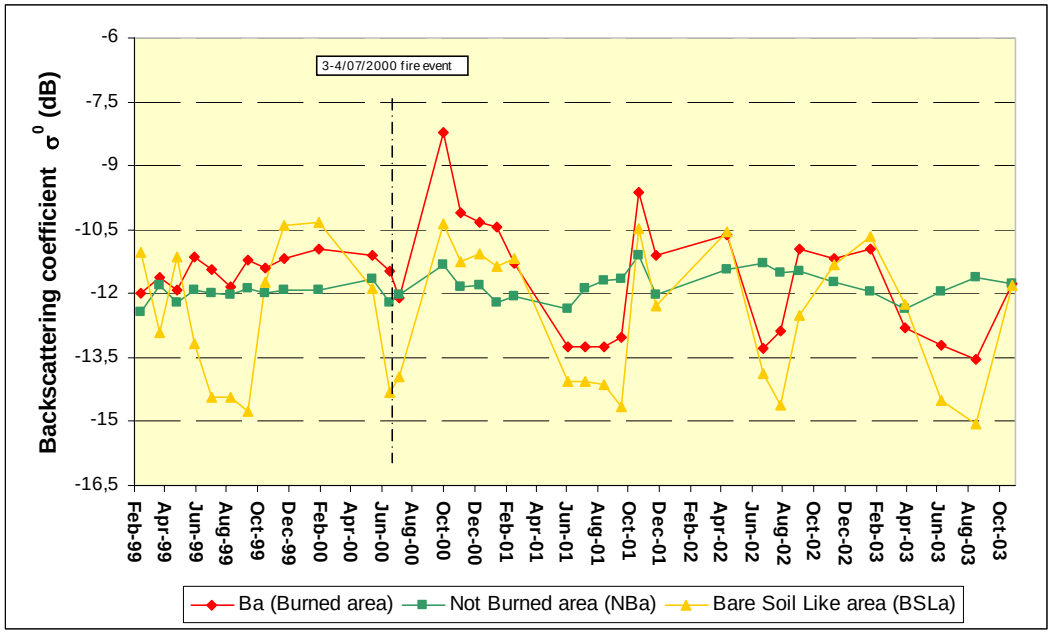

Fig. 4.4 Time behaviour of backscattering corresponding to the three main regions *Ba*, *NBa* and *BSLa*

Different comments are suggested by Fig. 4.4. The first one is on the behaviour of the *Bare Soil Like area*. It is clear how the seasonal cycle of the soil moisture drives the behaviour of the backscattering in the five considered years.

Particularly, it is interesting to observe the 5 peaks of low values, regularly occurring in the summer season, when the dielectric characteristics of the soil are described by low values of the soil moisture and, hence, of the dielectric constant. On the other hand, the backscattering time sequence of the pinewood region not affected by the fire event (*Not Burned area*) is much more stable with smaller fluctuations (less 1db) which may be scarcely correlated to the soil moisture values. Concerning the time behaviour of the *Burned area*, it's possible to separate among three different phases.

Before the fire event, the behaviour tends obviously to be closer to that of the *Not Burned area*, right after the event becomes closer to the *Bare Soil Like area* behaviour. In the period corresponding to the last two years, the similarity to bare soil seems to decrease as visible in Fig. 4.4 and Fig. 4.5 where the $\sigma^0 - <\sigma^0>$ profiles calculated for *Burned area* and *Bare Soil Like area* are compared.

The previous results suggest a possibility for monitoring the pinewood in the burned regions.

This might consist in tracking how much the backscattering behaviour of the burned region is similar to the backscattering of the bare soil region. In particular, a measure of this similarity could be represented by the evaluation, in the region to be monitored, of the annual backscattering excursion from the positive peak to the negative peak and comparing it to the one corresponding to the bare soil area.

The annual peak-to-peak transitions (occurring in a time window from February 1999 to October 2003) of backscattering have been considered and the backscattering difference for each transition has been also calculated for *Ba*, for *BSLa* and for *NBa*.

The results are shown in Table 3: the values of the first and second lines correspond to the transitions considered before the fire event, the third line to the transition right after the fire event, the others line to the transitions occurring in the following three years.

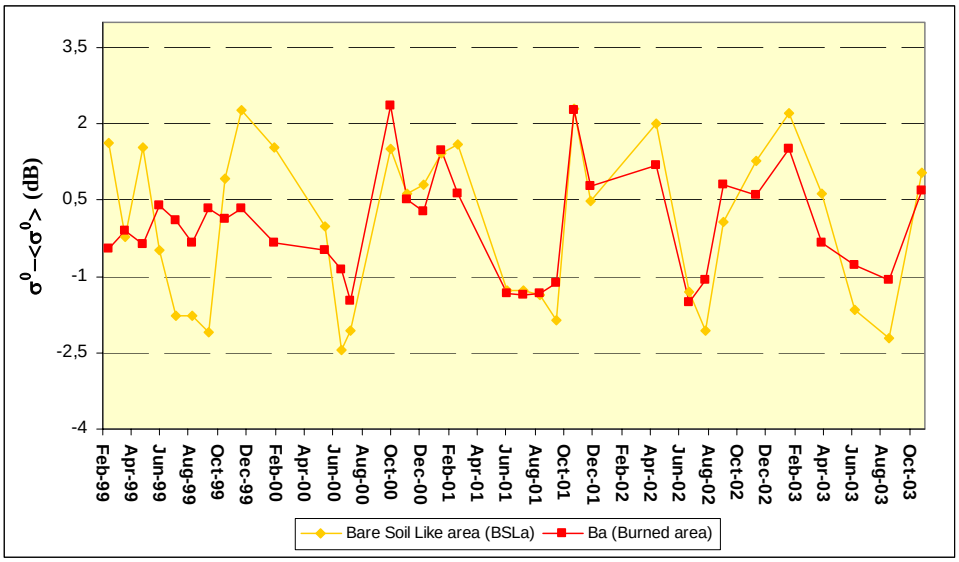

Fig. 4.5 σ^0–$<\sigma^0>$ profiles relatively to ***Burned area*** and ***Bare Soil Like area***

***Annual peak-to-peak backscatter transition* (dB)**	***Ba***	***BSLa***	***NBa***
1999	0,84	4,36	0,64
From January 2000 to June 2000 before the fire event	0,51	3,97	0,56
From July 2000 to December 2000 after the fire event	3,85	3,58	0,72
2001	3,66	4,52	1,26
2002	2,69	4,06	0,43
2003	2,58	4,42	0,72

Table 3 The annual peak-to-peak transitions (from February 1999 to October 2003) of backscattering relatively to the *Burned area*, *Bare Soil Like area* and *Not Burned area*

The histogram of Fig. 4.6 calculated from Table 3 shows that the values of transitions corresponding to the *BSLa* are the greatest in every year except for the

value right after the fire event. The transitions' values of the *NBa* are lower and seem to be rather uncorrelated with those of the bare soil.

Concerning the *Ba*, before the fire event, the difference respect to *BSLa* is rather high, about -3.5 dB, soon after the fire event becomes positive, but it starts progressively to decrease in the following three years.

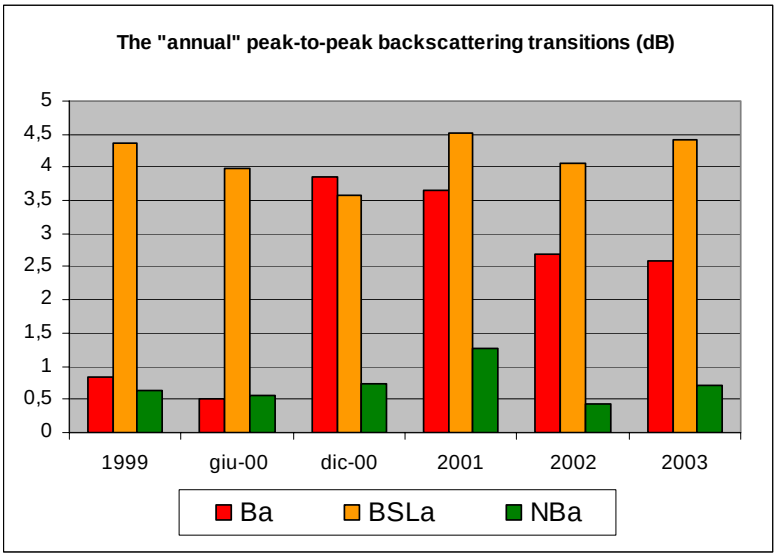

Fig. 4.6 The histogram represents the annual excursions of the backscattering coefficient relatively to *Ba*, *BSLa* and *NBa* regions

This behaviour suggests the possibility to measure the rate of the vegetation after the fire providing a reforestation index for the early years after a fire event. This reforestation index, that is the result of the difference between the annual backscattering excursion of *Ba* and *BSLa*, is showed in the following histogram of Fig. 4.7.

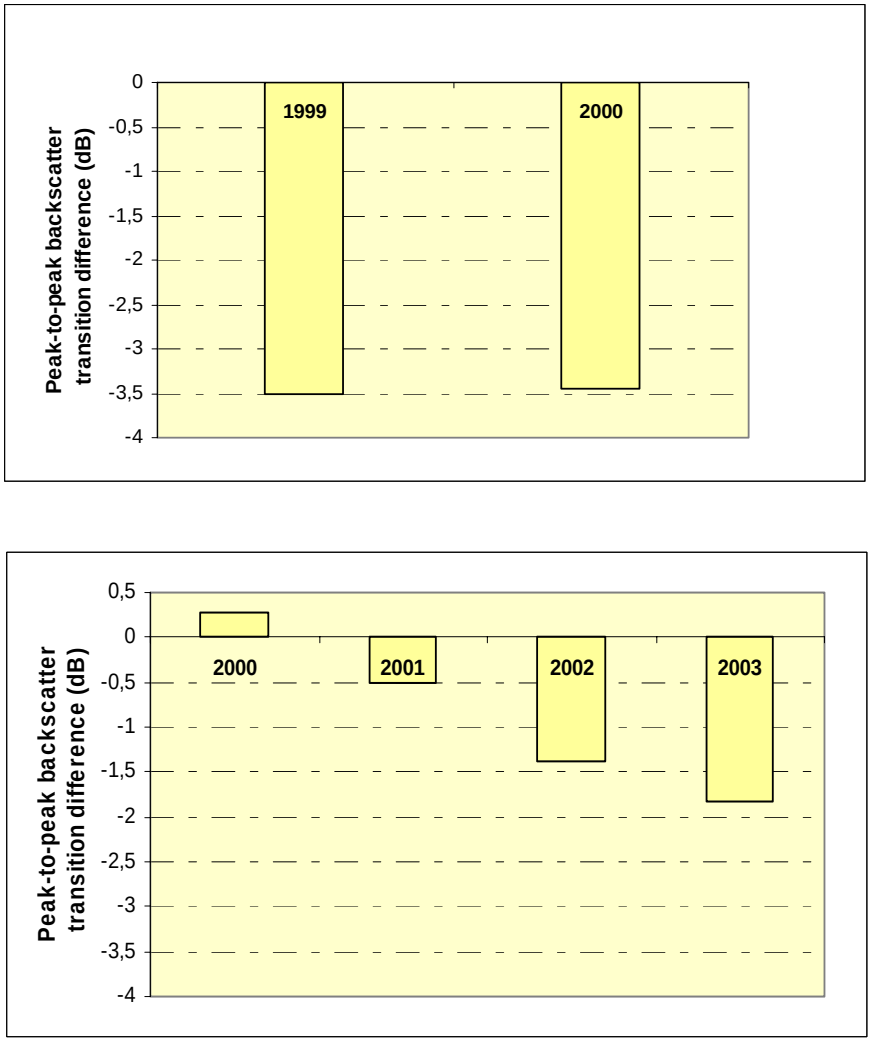

Fig. 4.7 Reforestation index: peak to peak backscatter transition difference histogram between the ***Ba*** and ***BSLa*** before (above diagram) and after the fire event (below diagram).

4.3 More specific result for the *burned area*

As reported in Table 2, inside the burned area it has been possible to make an additional distinction among the areas which were burned. In particular, two subsets of areas can be considered:

1. a subset composed by areas (**ab1**, **ab2**, **Alotto2**, **AS**) which underwent artificial interventions of reclaiming/plantation, although in different times. In Fig. 4.8 is reported the time behaviour of backscattering

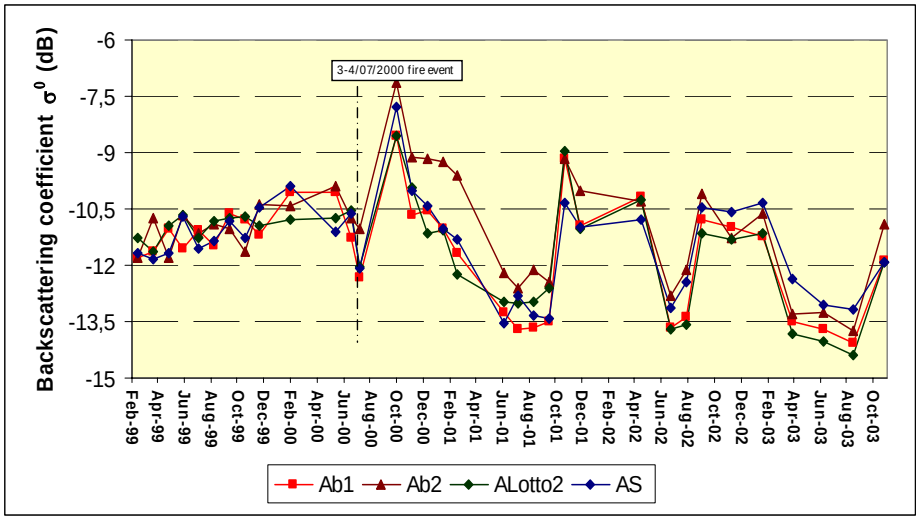

Fig. 4.8 Time behaviour of backscattering of ab1, ab2, ALotto2 and AS areas

2. a subset composed by areas (**AT**, **APG**, **ATP**, **A77-00**) where the process of growing has been completely spontaneous with no man made actions. In Fig. 4.9 is reported the time behaviour of backscattering

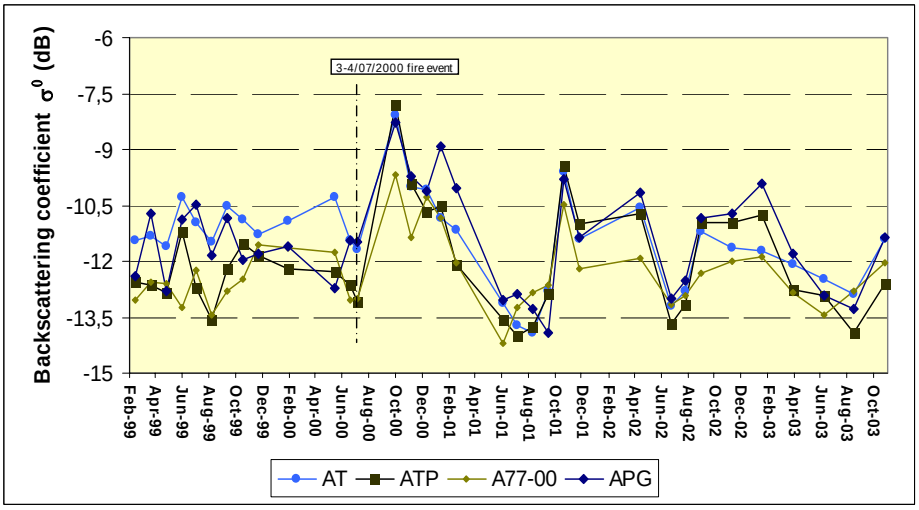

Fig. 4.9 Time behaviour of backscattering of AT, APG, ATP and A77-00 areas

If a comparison on the backscattering coefficient trend calculated considering the average areas for each of these two subsets is performed, the result is particularly interesting as it is possible to see in Fig. 4.10.

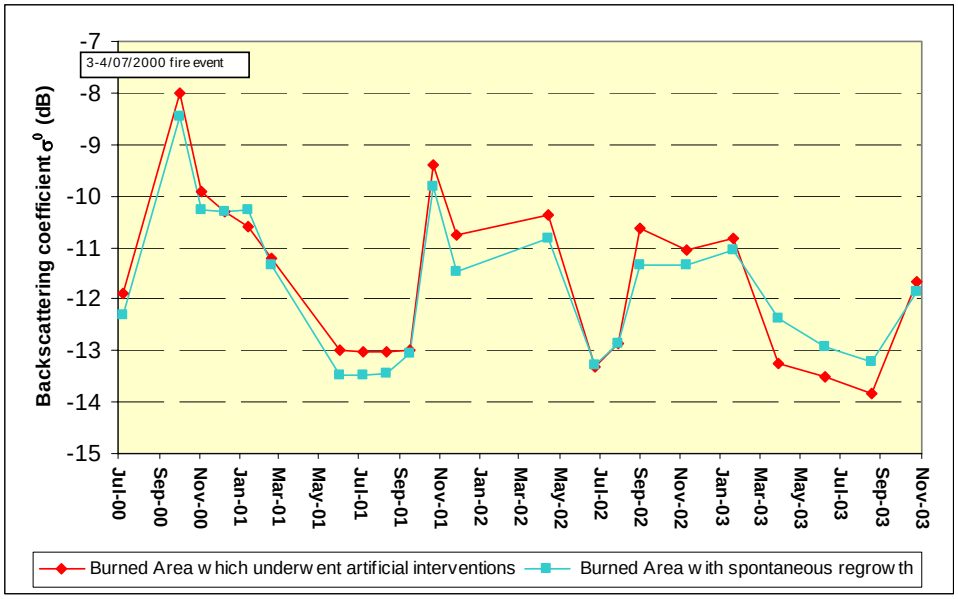

Fig. 4.10 Time behaviour of backscattering coefficient after the fire event calculated considering: a) the average area, called "*Burned Area which underwent artificial interventions*" (in red color) for the subset composed by burned areas which underwent artificial interventions of reclaiming/plantation; b) the average area, called "*Burned area with spontaneous* " (in blue color), of the other subset formed by areas where the process of growing has been completely spontaneous.

The two backscattering trends are similar in the first year after the fire but they become different especially in last year. Applying the same method used for the retrieval of the reforestation index to these two subsets, the trends showed in Fig. 4.11 have been obtained: the index shows a different rate of growing of the vegetation after the fire. In particular the growth has been greater in areas with spontaneous growing than in areas which underwent artificial interventions. These results are in agreement with the vegetation trends measured in situ by some researchers of the Faculty of Plant Biology of "La Sapienza" University.

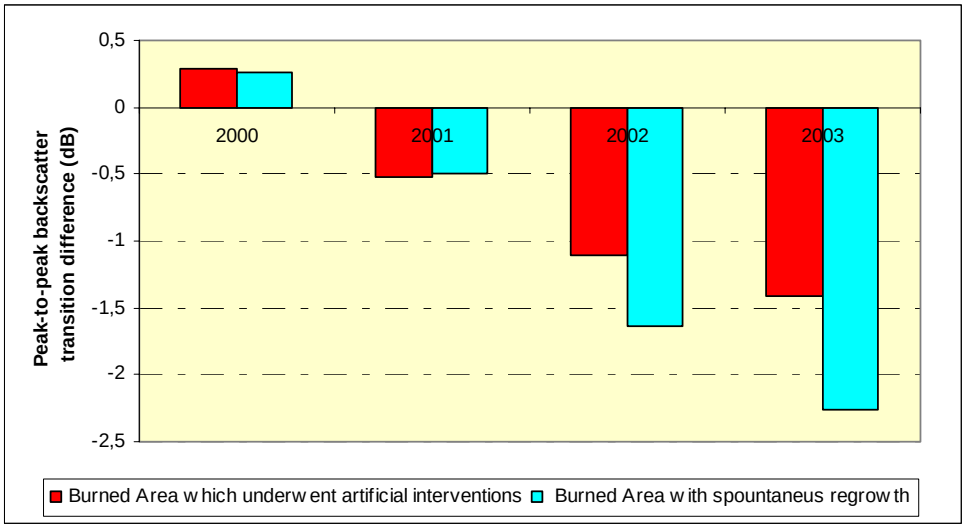

Fig. 4.11 Reforestation index: comparison between peak to peak backscatter transition difference of the *Burned area* that underwent artificial interventions and *Bare Soil Like area*, and peak to peak backscatter transition difference of *Burned area* with spontaneous and *Bare Soil Like area*, after the fire event

The reclamation process had an important "role" in starting reforestation development. The histogram of Fig. 4.11 shows that in 2001 the values of areas that underwent the reclamation and those corresponding to other areas are similar while one could expect a smaller (or even absent) regrowth in the reclaimed area. This could be explained by the fact that, in the year following the fire, the effects of the dramatic change of the landscape may in general contribute with different noises to the backscattering measurements.

Moreover, it should be considered that other sources of noise derive from the reclaiming process such as the presence of tractors and other garden machines, and of the operations of cutting and removal of burned biomass, which have modified the surface roughness and the soil characteristics. As also indicated by the figure, this type of noise should be less present in years 2002-2003.

As reported in Table 2, the reclaiming process can be considered almost completed at the end of summer of 2001. The above considerations lead to say that 2001 is a

particular year that has to be checked very carefully. Following in Fig. 4.12 and in Fig. 4.13, there some photos that suggest an idea about the stage of development of the vegetation inside the burned area

Fig. 4.12 Two photos of the area which *underwent artificial interventions of reclaiming and plantation* after 16-17 months (above) and after 40 months (below) from the fire

Fig. 4.13 Two photos of the area where the *process has been completely spontaneous* after 9-10 months (on the left) and after 40 months (on the right) from the fire growing process

Chapter 5 Biomass retrieval by means of a scattering model

5.1 Introduction

In the previous section, a qualitative index of the reforestation process of the burned area using multitemporal ERS-SAR data has been proposed. This index is based on the measurement, taken throughout at least one year, of the similarity between the backscattering of the burned area and the backscattering of a bare soil around or inside the burned area. In the present chapter an electromagnetic model has been used for a quantitative retrieval of biomass rate (ton/ha per year) after the fire inside the burned area where the reforestation process has been spontaneous. The retrieval of biomass trend has been performed by means of the "Water Cloud" model calibrated using some routines of the more complex Tor Vergata scattering electromagnetic model. The annual rate of growing is in agreement to the ground measurements collected by some researchers of the Plant Biology faculty of "La Sapienza" University in Rome.

5.2 Calibration of the Water Cloud model using the scattering model of "Tor Vergata"

As previously introduced in section 2.3, starting from the "Water Cloud" model expression for $\sigma^0_{can}(\vartheta)$,

(2–24) $\sigma^0_{can}(\vartheta) = c\left(1 - \exp(-d \cdot w)\right) + \sigma^0_s \exp(-d \cdot w)$

the coefficients ***c*** and ***d*** have been calculated using some routines of the Tor Vergata" discrete element scattering model. Before to explain the hypothesis assumed to calculate these coefficients, it is important to specify what is the target on which the biomass retrieval is done.

After very severe fire, the pinewood structure is almost totally destroyed, above all the underbrush, as visible in Fig. 3.2. Soon after the fire, even if some new branches come up from the few survived trees (Pinus pinea and Quercus ilex), the vegetation cover consists in general of shrubs and in this particular case of Mediterranean shrubs like Phillyrea latifoglia L., Pistacia lentiscus L., Cistus.

Hence, the target, that has to be considered, is composed by tall bushes that cover the terrain (and not trees).

5.2.a The assumed hypotheses

According to section 2.4.a, to calculate the coefficients ***c*** and ***d*** with the Tor Vergata model two hypotheses have been assumed: one related to the vegetation development and the other related to the water content of the vegetation and the dimension of branches.

With reference to first one, canopies uniformly filled with equal cylinders have been considered; it has been supposed that the radius of cylinders grows up from 0 cm to 0,5 cm, starting the process soon after the fire till October 2003. The variation is a linear variation relative to the time as showed in Fig. 5.1.

These values are in agreement with the experimental data available at "La Sapienza" University, Rome, Biology department, considering the Mediterranean vegetation types present in the Castel Fusano area after the fire and the collections of ground measurements reported in [47]. It has to be noticed that for the 2003 the increase of radius is not the same of the years before. During 2003, indeed, there was a very dry summer without rain for more than four months (from May to the first days of September) and this element has been considered in the hypothesis of development, considering a smaller growth for the summer months.

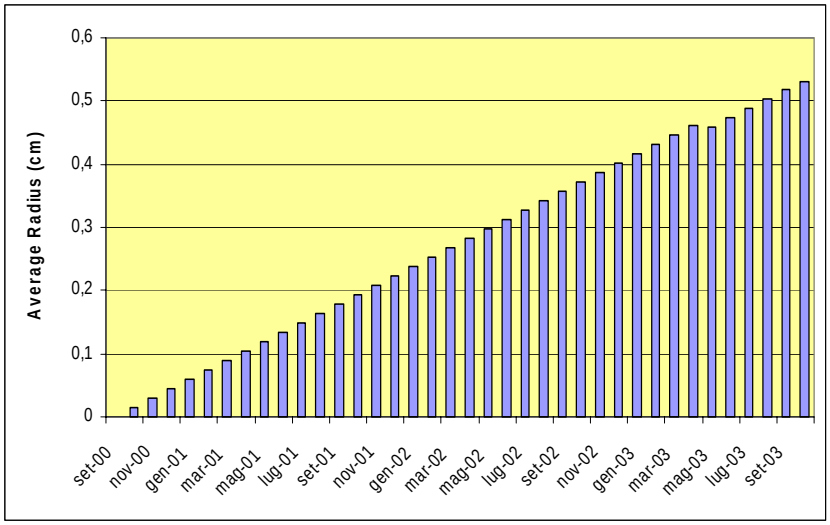

Fig. 5.1 Dimensions of cylinder average radius considering a linear development of the canopy respect to the time.

Concerning the plant water content it has been assumed equal to 70% by weight and the cylinder length has been fixed to 50 times the radius dimension.

Making these hypotheses and assuming the characteristic parameters of frequency and incidence angle of ERS1-2 satellite, the coefficient ***c*** and ***d*** have been calculated (see Table 4). For each supposed radius value, the coefficients are the result of an average operation supposing a range composed by 4 values bigger and 4 smaller than the hypothesize radius. For example if the supposed radius dimension is equal to 0,21 cm, the coefficients *c* and *d* are the average of the coefficients relative to the range [0,17-0,25] cm.

With reference to the contribution σ_s^0 coming from the soil, the measured values of backscattering relative to *Bare Soil Like area* have been implemented.

The last hypothesis is on the rate of regrowing. It has been assumed that the growth rate of biomass (ton/ha per year) is constant during the year and the same for the entire time period of analysis (2001-2003).

height (cm)	radius (cm)	total weight (g)	dry weight (g)	c	d (m^2/kg)
0,5	0,01	0	0	0	0,38
1	0,02	0,001	0	0,003	0,398
1,5	0,03	0,002	0,001	0,01	0,426
2	0,04	0,006	0,002	0,02	0,466
2,5	0,05	0,012	0,003	0,033	0,519
3	0,06	0,02	0,006	0,048	0,587
3,5	0,07	0,032	0,01	0,064	0,672
4	0,08	0,047	0,014	0,08	0,775
4,5	0,09	0,067	0,02	0,097	0,896
5	0,1	0,092	0,028	0,112	1,033
5,5	0,11	0,123	0,037	0,125	1,178
6	0,12	0,16	0,048	0,136	1,323
6,5	0,13	0,203	0,061	0,143	1,453
7	0,14	0,254	0,076	0,148	1,557
7,5	0,15	0,312	0,094	0,15	1,627
8	0,16	0,378	0,114	0,149	1,661
8,5	0,17	0,454	0,136	0,147	1,663
9	0,18	0,539	0,162	0,144	1,639
9,5	0,19	0,634	0,19	0,14	1,599
10	0,2	0,739	0,222	0,136	1,549
10,5	0,21	0,856	0,257	0,132	1,493
11	0,22	0,984	0,295	0,128	1,436
11,5	0,23	1,124	0,337	0,124	1,38
12	0,24	1,277	0,383	0,12	1,328
12,5	0,25	1,444	0,433	0,116	1,28
13	0,26	1,624	0,487	0,113	1,238
13,5	0,27	1,819	0,546	0,109	1,201
14	0,28	2,028	0,609	0,106	1,17
14,5	0,29	2,254	0,676	0,102	1,147
15	0,3	2,495	0,748	0,097	1,131
15,5	0,31	2,753	0,826	0,092	1,123
16	0,32	3,028	0,908	0,087	1,122
16,5	0,33	3,321	0,996	0,082	1,128
17	0,34	3,632	1,09	0,077	1,138
17,5	0,35	3,962	1,188	0,071	1,15
18	0,36	4,311	1,293	0,065	1,16
18,5	0,37	4,68	1,404	0,058	1,166
19	0,38	5,07	1,521	0,052	1,163
19,5	0,39	5,481	1,644	0,046	1,148
20	0,4	5,914	1,774	0,04	1,119
20,5	0,41	6,368	1,91	0,035	1,076
21	0,42	6,846	2,054	0,032	1,02
21,5	0,43	7,346	2,204	0,03	0,954
22	0,44	7,871	2,361	0,032	0,884
22,5	0,45	8,42	2,526	0,035	0,814
23	0,46	8,994	2,698	0,039	0,748
23,5	0,47	9,593	2,878	0,045	0,688
24	0,48	10,219	3,066	0,051	0,634
24,5	0,49	10,871	3,261	0,058	0,586
25	0,5	11,55	3,465	0,065	0,544

Table 4 Table of coefficients *c* and *d*, calculated using some routines of the Tor Vergata Model

5.3 The simulation and the retrieval

According to the previous hypotheses, the model has been implemented considering a parametric variation of the rate of biomass per year (ton/ha per year) and hence of the content of water *w* inside the vegetation.

Analysing the first results of the simulations, an example is reported in Fig. 5.2, a bias (about 0.4 dB) between the predicted and measured curve was evident.

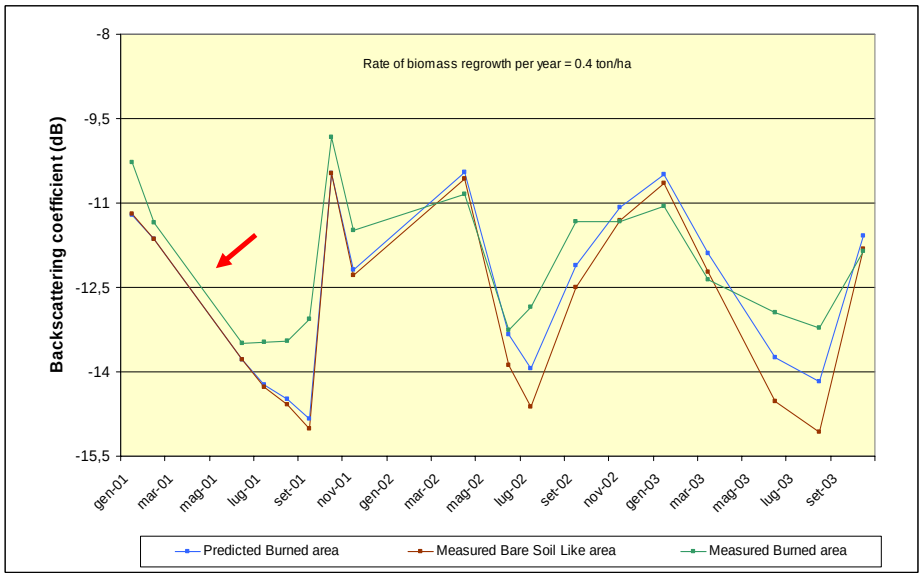

Fig. 5.2 Example of simulation: a bias between the predicted and measured curve is evident.

Because of that, a correction of this bias has been implemented in the model, as showed in Fig. 5.3. For each considered value of biomass, the RMS error between the predicted and measured values of σ^0_{can} has been calculated

$$RMSe = \sqrt{\frac{\sum_{i=1}^{N}\left(\sigma^{0}_{can-predicted}{}^{(i)} - \sigma^{0}_{can-measured}{}^{(i)}\right)^2}{N}} \quad (5\text{–}1)$$

where i =1….N is the time date acquisition.

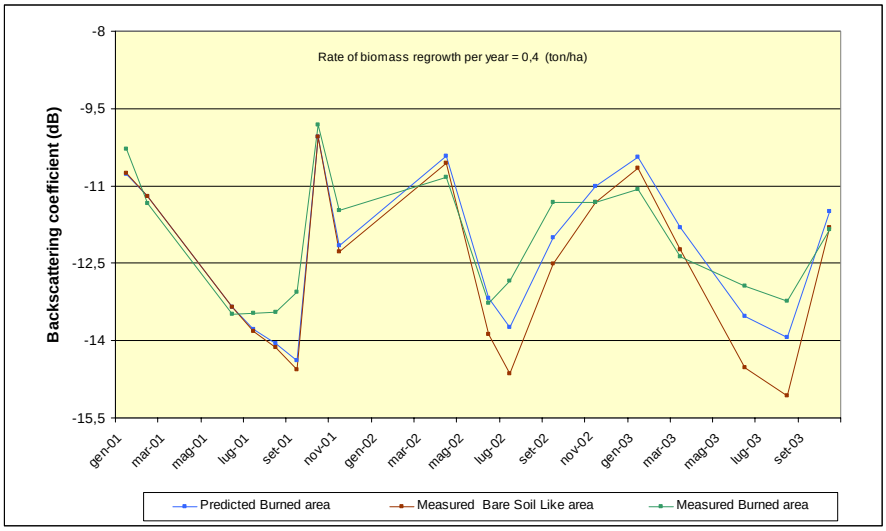

Fig. 5.3 Example of simulation after bias correction.

In Fig. 5.4 is showed the RMS error (dB) diagram relatively to the 2001-2003 period. The minimum of the curve is in association with the value of 0,85 ton/ha year.

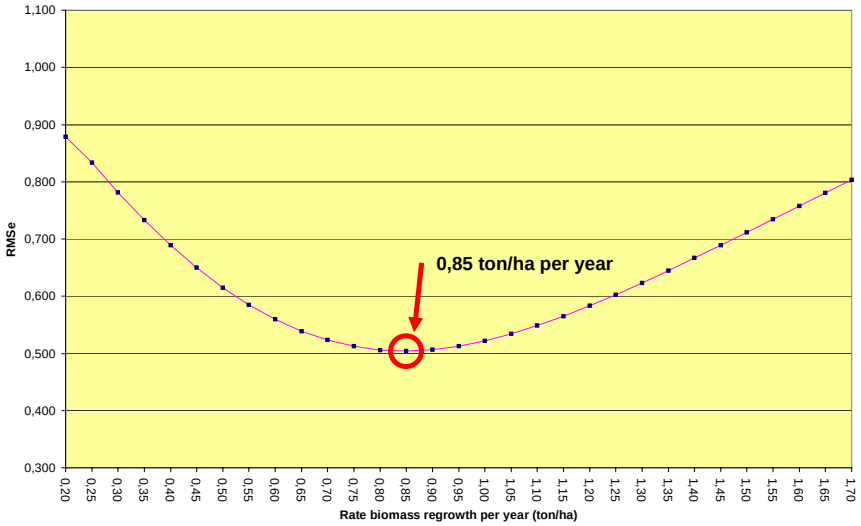

Fig. 5.4 RMSe diagram calculated considering the predicted and measured values of σ^0_{can} relatively to 2001-2003 time period

The RMSe diagram has been computed also referring to only 2002-2003 time period (Fig. 5.5). In this case the minimum value of the curve is 0.8 ton/ha per year.

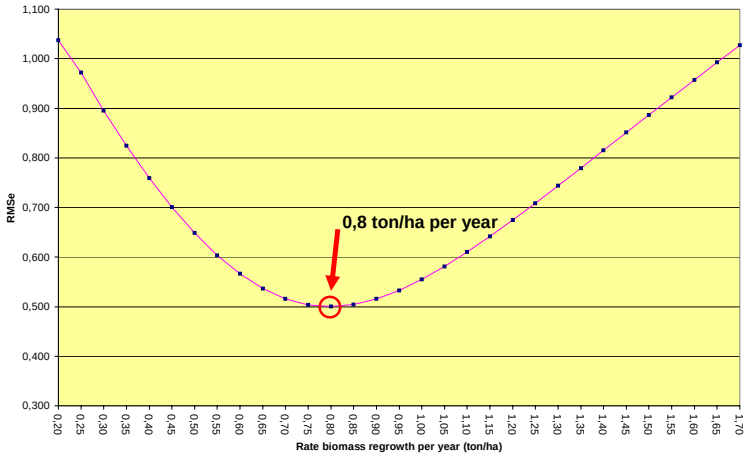

Fig. 5.5 RMSe diagram calculated considering the predicted and measured values of relatively to 2002-2003 time period

The backscattering predicted trend corresponding to the biomass value of 0,8 ton/ha per year is shown in Fig. 5.6 together with the measured trend.

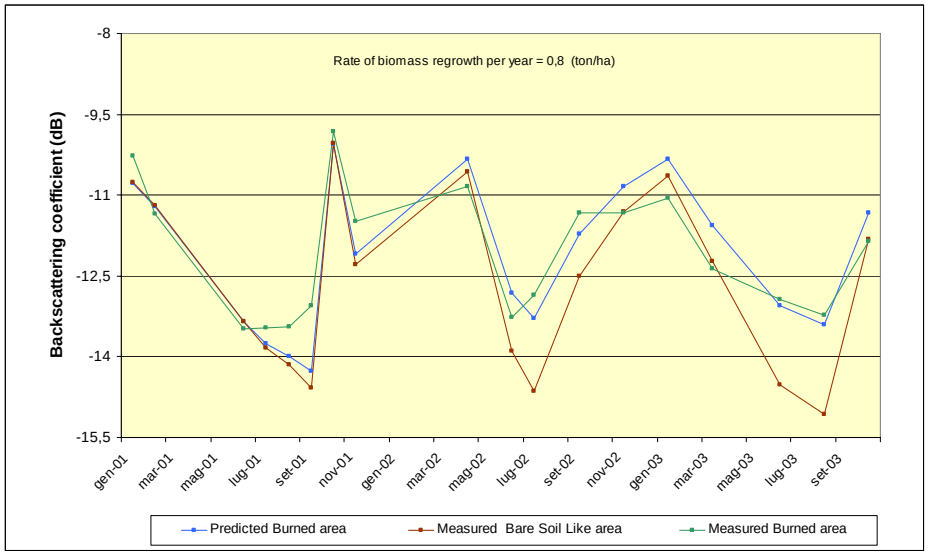

Fig. 5.6 Backscattering predicted trend relatively to the rate of biomass of 0.8 ton/ha per year

The RMSe curve relatively to the 2001-2003 period has the minimum in correspondence of 0.85 ton/ha per year but the sensitivity of the curve is not so good. On the contrary, if we consider the curve relatively to 2002-2003 time period, the minimum is the value of 0.80 ton/ha per year but the curve shows a better sensitivity than in the previous time period.

This could be due to the noise of terrain changes caused by fire, which in general are present in the following year after the fire. This noise is less present after the first year and this could explain the better sensitivity in 2002-2003.

The retrieved rate of 0.80 ton/ha per year is a reasonable value, as the biologists of "La Sapienza" University have confirmed from their ground measurements and from [47].

Chapter 6 Conclusion

The following conclusions can be drawn at the end of this thesis work.

- A multitemporal analysis of the backscattering coefficient measured over the Castel Fusano pinewood, partially destroyed in a fire event of July 2000, has been carried out using C band ERS SAR data. The time period of analysis is more of three years.

- The retrieval of the fire scar does not seem to be feasible with one ERS SAR image. However, due to the increased influence of soil moisture in the backscattering, the fire scar might be detected with multitemporal measurements taken on the same season.

- The measurement, taken throughout at least one year, of the similarity between the backscattering of the burned area and the backscattering of a bare soil around or inside the burned area, provide a qualitative index of the reforestation process of the burned area permitting a separation among the area with spontaneous re-growth and the one which underwent man made interventions.

- The retrieval of biomass rate of growing (ton/ha per year) after the fire, inside the area where the regrowing process has been spontaneous, has been performed by means of the “Water Cloud” model calibrated using some routines of the Tor Vergata scattering electromagnetic model: the retrieved value is in agreement to what measured by some researchers of Plant Biology faculty of “La Sapienza” University

In appendix we have been briefly reported the results of two different studies employing other data. The first study is on the impact of different polarization and different incidence angle on backscattering, employing APP VV-VH IS4 ASAR Envisat data. The other study employs Landsat data over the same period of ERS SAR data: the NDVI shows a similar trend to that of the index of reforestation process defined employing SAR images till 2002, but no conclusion can be pronounced about 2003.

Appendix Use of other data: SAR multipolarized and Optical

A.1 ASAR Envisat

To evaluate the effects of incidence angle and polarization on the sensitivity of backscattering coefficient, an additional exercise, employing ERS and ASAR images, has been carried out.

In particular the comparison between the behaviour of backscattering coefficient of ASAR IMP IS1, ASAR APP IS4 and ERS images has been considered. The images have been all acquired in March 2003 but in different days: ASAR IMP IS1 has been acquired the 14th march 2003, ASAR APP IS4 VV-VH has been acquired the 27th March 2003 and ERS SLCI has been acquired the 30th March 2003

It is important to keep in mind the different incidence angle ranges: the incidence angle range for the IS1 ASAR swath goes from 14.1 to 22.3 degrees, for IS4 ASAR from 30.6 to 36.2 degrees and at last for ERS from about 20 degrees to 26 degrees. Moreover, the APP image is an alternative polarization VV-VH configuration so it has been possible to formulate a first valuation of the impact of two different polarizations on the backscattering values.

Before illustrating these preliminary results, it has to underlined that during the acquisition on 14 March 2003 there was slight rain, instead concerning the other two acquisitions, the weather conditions in the last week of March were stable without rain [46].

The analysis has been carried out using the four macro-regions of interest which are the “Not Burned area”, the “Burned area that underwent artificial interventions of reclaiming”, the “Burned area without any interventions man made” and the “Bare Soil Like area” (see sections 3.3 and 4.3).

Table 5 and Fig A.1 show the backscattering values calculated on each area and considering different acquisition modes.

Acquisition date	Sensor	Not Burned area	Burned area with interventions	Burned area without interventions	Bare Soil Like area
14-Mar-03	ASAR VV IS1	-11.72 dB	-11.50 dB	-11.27 dB	-11.18 dB
27-Mar-03	ASAR VV IS4	-10.79 dB	-11.97 dB	-11.50 dB	-10.89 dB
27-Mar-03	ASAR VH IS4	-15.92 dB	**-18.10 dB**	**-17.17 dB**	-16.09 dB
30-Mar-03	ERS VV	-12.34 dB	**-13.24 dB**	**-12.36 dB**	-12.23 dB

Table 5 Backscattering values calculated considering each macro-region and the acquisition mode.

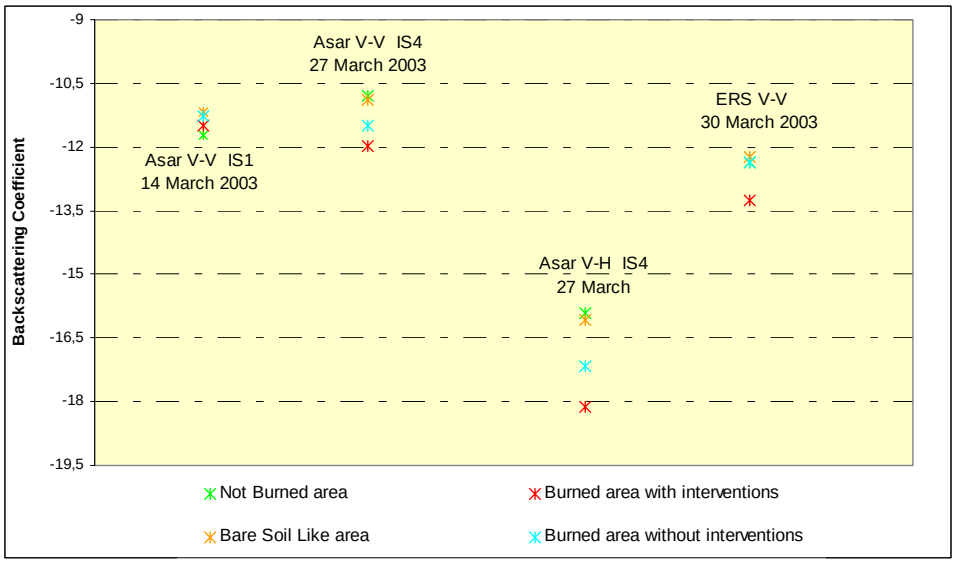

Fig. A1 Backscattering values of each macro-region and the acquisition mode versus time

In Table 6, the backscattering signal excursion for each date and taking into consideration all the regions is reported.

		MIN (dB)	MAX (dB)	Δ(MAX-MIN) (dB)
ASAR VV IS1		-11.72	-11.18	0.53
ASAR VV IS4		-11.97	-10.79	1.17
ASAR VH IS4		-18.10	-15.92	2.18
ERS VV		-13.24	-12,23	1,01

Table 6 Backscattering signal excursion for each date and taking into consideration all the four macro-regions

From these results some preliminary considerations could be done:

- VH polarisation: the min e max values are lower than the others and the dynamic range is the highest
- The IS4 incidence angle range seems to be more sensitive to discriminate different levels of vegetation on the terrain respect of ERS configuration
- Concerning IS1 the presence of rain during the acquisition doesn't allow confident considerations

Unfortunately, for the image acquisition policy of European Space Agency, we did not have at the moment other images available.

A.2 Landsat TM

A study on the area of Castel Fusano employing Landsat TM images in collaboration with the Departement of Plant Biology of "La Sapienza" University has been carried out. Five Landsat TM images all acquired in the summer period (July-August) from 1999 to 2003, before and after the fire event have been used, and the same areas considered in the SAR analysis have been employed (see sections 3.3 and 4.3). Different index like NDVI (normalized difference vegetation index), MSI (Moisture Stress Index), TM3/TM2, NBR (Normalized Burn Ratio), RI (Regeneration Index) have been calculated. In Fig. A.2, the NDVI index for the *Burned area (Ba)*, the *Bare Soil Like area (BSLa)* and the *Not Burned area (NBa)* is calculated.

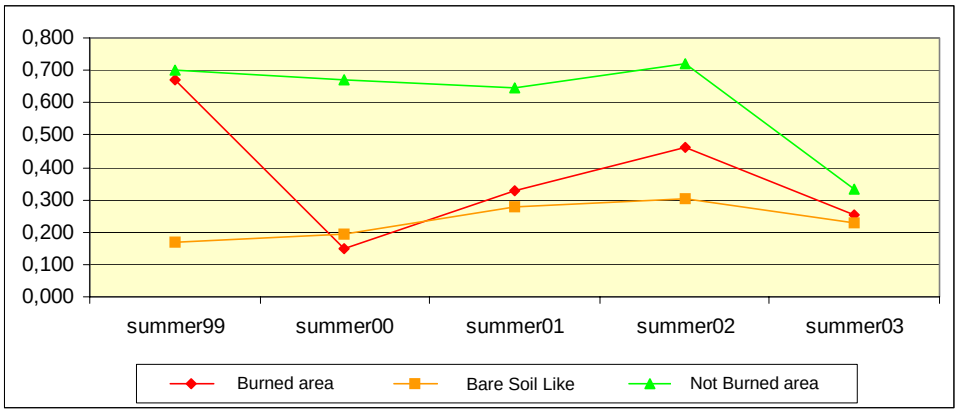

Fig. A.2 NDVI index for the Burned area (Ba), the Like Bare Soil area (Bsla) and the Not Burned area (NBa).

Before the fire event, the *Burned area* and the *Not Burned area* have similar values of NDVI and furthermore very different from that of *Bare Soil Like area*. After one year from the fire event, in 2001, the NDVI of the *Ba* is close to that of *BSLa* but already shows a little difference with the last one. This difference still grows more in 2002, but in 2003 collapses, as if another fire event happened. Really the summer of 2003 was a very dry season (it hasn't rain from May to the end of August) and this has caused a reduction of active biomass in photosynthesis

process. This effect of strong moisture stress prevents the possibility to confirm the 2003 further growth in the area under analysis, as reported by the ground measurements campaign made by the biologists. If we distinguish inside the burned area the area that underwent manmade interventions from that where the re-growth has been spontaneous, the NDVI trends calculated on these areas, showed in Fig. A.3, confirm that the vegetation development in the area with no interventions has been greater than the reclaimed one till 2002, but nothing could be said on 2003 values.

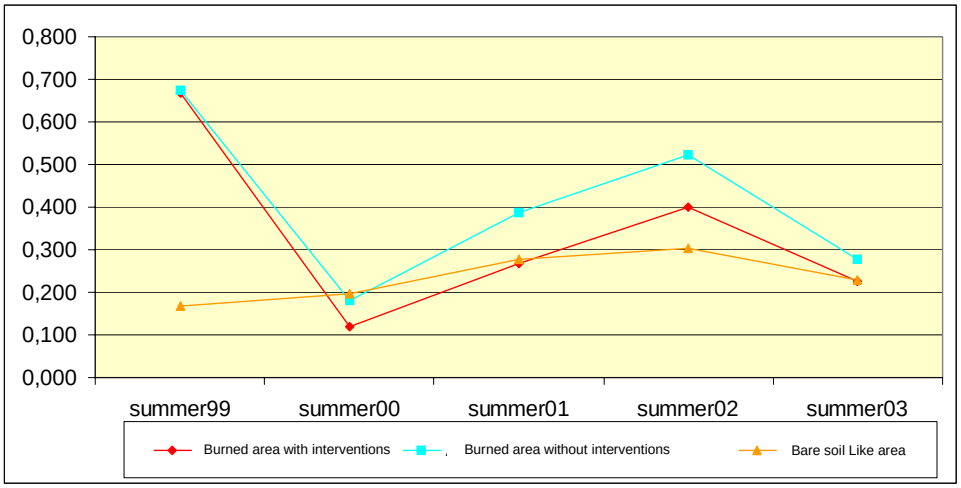

Fig. A.3 NDVI index calculated relatively to Burned area with artificial interventions and without interventions and Bare Soil Like area.

List of Figure

List of Tables

References

[1] R. J. E. Brown *"Effects of Fire on the Permafrost Ground Thermal Regime"*, in Wein R. W. and Maclean. A. (Ed.) "The Role of Fire in Northern Circumpolarcosystems" John Wiley & Sons, New York, pp. 97-110, 1983

[2] C. Justice and S. Korontzi *"A review of satellite fire monitoring and the requirements for global environmental change research"*, in "Global and Regional Wildland Fire Monitoring from Space: Planning a Coordinated International Effort", pp. 1-18, (2001)

[3] V. A. Alexeyev and R. A Birdsey *"Carbon in Ecosystems of Forests and Peatlands of Russia"*, Jove Loony, Krasnoyarsk, Syberia, pp. 170, 1994

[4] J. S Levine and W. R. Cofer, III, *"Boreal forest-re emissions and the chemistry of the atmosphere"*, in Fire, Climate Change, and Carbon Cycling in the North American Boreal Forest, edited by E. S. Kasischke and B. J. Stocks (New York: Springer-Verlag), pp. 31–48., 2000

[5] D. I. Odintsov *"Fire Prevention"* Forest Management, Vol. 3, pp. 2-4, 1996

[6] K. J Ranson., G. Sun, K. Kovacs, V. I. Kharuk *"MODIS NDVI Response Following Fires in Siberia"*, Geoscience and Remote Sensing Symposium, 2003, IGARSS '03. Greenbelt, MD, USA. 21-25 July 2003

[7] Z. Li, J. Cihlar, L. Moreau, F. Huang, and B. Lee, *"Monitoring fire activities in the boreal ecosystem"*, J. Geophys. Res., vol. 102, pp. 29611–29624, 1997

[8] Z. Li, S. Nadon, J. Cihlar, and B. Stocks, *"Satellite-based mapping of Canadian boreal forest fires: Evaluation and comparison of algorithms"*, Int. J. Remote Sens., vol. 21, pp. 3071–3082, 2000

[9] D. R. Cahoon, B. J. Stocks, J. S. Levine, W. R. Cofer and C. C. Chung, *"Evaluation of a technique for satellite-derived area estimation of forest fire"*, J. Geophys. Res.-Atmos., vol. 97, pp. 3805–3814, 1992

[10] E. S. Kasischke, N. H. F. French, P. Harrell, N. L. Christensen, S. L. Ustin and D. Barry, *"Monitoring of wildfires in boreal forests using large-area AVHRR NDVI composite image data"* Remote Sens. Environ., vol. 45, pp. 61–71, 1993

[11] P. M. Barbosa, J. M. Gregoire and J. M. C. Pereira, *"An algorithm forextracting burned areas from time series of AVHRR GAC data applied at a continental scale"*, Remote Sens. Environ., vol. 69, pp. 253–263, 1999

[12] R. H. Fraser, Z. Li, and J. Cihlar, *"Hotspot and NDVI differencing synergy (HANDS): A new technique for burned area mapping over boreal forest"*, Remote Sens. Environ., vol. 74, pp. 362–376, 2000

[13] K. R. Al-Rawi, J. L. Casanova, and A. Romo, *"IFEMS: A new approach for monitoring wildfire evolution with NOAA-AVHRR imagery"*, Int. J. Remote Sens., vol. 22, pp. 2033–2042, 2001

[14] O. Arino, I. Piccolini, E. Kasischke, F. Siegert, E. Chuvieco, P. Martin, Z. Li, R. Fraser, H. Eva, D. Stroppiana, J. Pereira, J. M. N. Silva, D. Roy, and P. Barbosa, *"Burn scar mapping methods"*, in Forest Fire Monitoring and Mapping: A Component of Global Observation of Forest Cover, ser. Environment and the Quality of Life Series, F. Ahern, J. J. Gregoire, and C. J. Justice, Eds: Eur. Commission, vol. EUR 19588 EN, pp.198–223, 2000

[15] Y. J. Kaufman, C. O. Justice, L. P. Flynn, J. D. Kendall, E. M. Prins, L. Giglio, D. E.Ward,W. P. Menzel, and A.W. Setzer, *"Potential global fire monitoring from EOS-MODIS"*, J. Geophys. Res-Atmos., vol. 103, pp. 32215–32238, 1998

[16] H. Eva and E. F. Lambin, *"Burnt area mapping in Central Africa using ATSR data"*, Int. J. Remote Sens., vol. 19, pp. 3473–3497, 1998

[17] Zhang Y. H., Wooster M. J., Tutubalina O. and Perry G. L. W., *"Monthly Burned Area and Forest Fire Carbon Emission Estimates for the Russian Federation from SPOT VGT"*, Remote Sensing of Environment, Vol.87, 1-15, 2003

[18] R. H. Fraser, Z. Li and R. Landry, *"SPOT VEGETATION for characterizing boreal forest fires"*, Int. J. Remote Sens., vol. 21, pp. 3525–3532, 2000

[19] M. C. Pereira and A. W. Setzer, *"Spectral characteristics of fire scars in Landsat-5 TM images of Amazonia"*, Int. J. Remote Sens., vol. 14, pp. 2061–2078, 1993

[20] E. Chuvieco and R. G. Congalton, *"Mapping and inventory of forest fires from digital processing of TM data"*, Geocarto International, 4, pp. 41–53, 1988

[21] V. Cuomo, R. Lasaponara, and V. Tramutoli, *"Evaluation of a new satellite-based method for forest fire detection"* Int. J. Remote Sens., vol. 22, pp. 1799–1826, 2001.

[22] Van Cleve, K. and Viereck, L. A., *"Forest succession in relation to nutrient cycling in the boreal forest of Alaska"*, in Forest Succession; Concepts and Application, edited by D. C. West, H. H. Shugart and D. B. Botkin, Chapter 13 (New York: Springer-Verlag), 1981

[23] Y. Zhang, P. Whitehead, W. Ahmad, and C. H Menges, *"An operational approach for mapping bushfire history in the tropical savannas of northern Australia"*, Proceedings of the 21st Asian Conference on Remote Sensing, Taipei, Taiwan, vol. I (Taipei, Taiwan: Asian Association on Remote Sensing), pp. 609–614, December, 2000

[24] L. L Bourgeau-Chavez., E. S. Kasischke, S. Brunzell and J. P. Mudd, *"Mapping Fire Scars in Global Boreal Forests Using Imaging Radar Data"*, International Journal of Remote Sensing, Vol. 23 (20), 4211-4234, 2002

[25] L. L. Bourgeau-Chavez, P. A Harrell, E. S. Kasischke and N. H. F. French, *"The Detection and Mapping of Alaskan Wildfires Using a Spaceborne Imaging Radar System"*, International Journal of Remote Sensing, Vol. 18, 355-373, 1997

[26] C. T. Dyrness and R. A. Norum, *"The Effects of Experimental Fires on Black Spruce Forest Floors in Interior Alaska"*, Canadian Journal of Forest Research, Vol. 13, 879-893, 2002

[27] S. Kuntz, F. Siegert and G. Ruecker, *"ERS SAR Images for Tropical Rainforest and Land Use Monitoring: Change Detection over Five Years and Comparison with Radarsat and JERS SAR Images"*, In Proceedings of IGARRS 1999, IEEE Geoscience and Remote Sensing Society, Piscataway, 1999

[28] F. Siegert and G. Rücker, *"Use of Multitemporal ERS-2 SAR Images for Identification of Burned Scars in South-East Asian Tropical Rain Forest"*, International Journal of Remote Sensing, Vol. 21(4), 831-837, 2000.

[29] M. Gimeno, J. San-Miguel, P. Barbosa and G. Schmuck, *"Using ERS-SAR Images for Burnt Area Mapping in Mediterranean Landscapes"*, in Viegas (Ed.), Forest Fire Research & Wildland Fire Safety, Mill press, Rotterdam, ,2002

[30] M. C. Dobson, F. T. Ulaby, T. Le Toan, **A.** Beaudoin, E. S. Kasischke, and N. Christensen, *"Dependence of radar backscatter on coniferous forest biomass"*, IEEE Trans. Geosci. Remote Sens., vol. 30, pp. 412-415, 1992.

[31] S. Couturier, S. Chin Liew, M. Nakayama and H. Lim *"Monitoring Vegetation Regeneration in Fire-Affected Tropical forest using ERS/JERS Synthetic Aperture Radar"*, IEEE Trans. Geosci. Remote Sens., vol. 24, pp. 560-571, 1999

[32] S. Huang, F. Siegert *"Envisat ASAR Wide swath Backscatter dynamics of the siberial boreal forest fire scar"* Proc. of the 2004 Envisat & ERS Symposium, Salzburg, Austria 6-10 September 2004 (ESA SP-572, April 2005)

[33] C. H. Menges, R. E. Bartolo, D. Bell and G. J. E. Hill *"The effect of savanna fires on SAR backscatter in northern Australia"*, INT. J. REMOTE SENSING, VOL. 25, NO. 22, 4857–4871, 2004

[34] T. Calvao and J. M. Palmeri, *"Mapping Mediterranean scrub with satellite imagery: biomass estimation and spectral behaviour"* INT. J. REMOTE SENSING, August, 2004, VOL. 25, NO. 16, 3113–3126

[35] F.Catalucci, F.Del Frate, A. Minchella, M. Paganini, *"Multitemporal ERS and ENVISAT Imagery for the estimation of the reforestation process of burned areas"*, Envisat & ERS symposium, Salzburg (Austria), 6-10 September 2004

[36] F. T. Ulaby, R. K. Moore, and A. K. Fung, *"Microwave Remote Sensing: Active and Passive"*, vol. II, Addison-Wesley, 1982

[37] P. Ferrazzoli and L. Guerriero *"Radar Sensitivity to Tree Geometry and Woody Volume: A Model Analysis"*, IEEE Trans. Geosci. Remote Sens., vol. 33, pp. 360-371, 1995

[38] P. Ferrazzoli, L. Guerriero, D. Solimini, *"Numerical model of microwave backscattering and emission from terrain covered with vegetation"*, Appl. Computat. Electromag. SOC. J., vol. 6, pp. 175-191, 1991

[39] S. Twomey, H. Jacobwitz, and H. B. Howell, *"Matrix method for multiple scattering problems"* J. Atmos. Sci., vol. 23, pp. 289-296, 1966

[40] H. J. Eom and A. K. Fung, *"A scatter model for vegetation up to Ku-band"*, Remote Sens. Environ., vol. 15, pp. 185-200, 1984

[41] R. Schiffer and K. 0. Thielheim, *"Light scattering by dielectric needles and disks"*, J. Appl. Phys., vol. 50, pp. 2476-2483, 1979.

[42] D. M. Le Vine, R. Meneghini, R. H. Lang, and S. S. Seker *"Scattering from arbitrarily oriented dielectric disks in the physical optics regime"*, J. Opt. SOC. Am., vol. 73, pp. 1255-1262, 1983

[43] M. A. Karam and A. K. Fung, *"Electromagnetic scattering from a layer of finite length, randomly oriented, dielectric, circular cylinders over a rough interface with application to vegetation"* Int. J. Remote Sensing, VOI. 9, pp. 1109-1 134, 1988

[44] M. A. El-Rayes and F. T. Ulaby, *"Microwave dielectric spectrum of vegetation-Part I: Experimental observations"*, IEEE Trans. Geosci. Remote Sens., vol. GRS-25, pp. 541-549, 1987.

[45] F. T. Ulaby, R. K. Moore, and A. K. Fung, *"Microwave Remote Sensing: Active and Passive (From theory to application)"*, vol. I, Reading, MA: Addison-Wesley, 1982

[46] http://www.wunderground.com

[47] L.F. Ohmann and D.F. Grigal *"Early revegetation and nutrient dynamics following the 1971 Little Sioux forest fire in north-eastern Minnesota"*, Forest Sci. Monogr. 21, 1979